

A THEORETICAL FRAMEWORK OF THE SCALED GAUSSIAN STOCHASTIC PROCESS IN PREDICTION AND CALIBRATION

BY MENG YANG GU , FANG ZHENG XIE AND LONG WANG

*Department of Applied Mathematics and Statistics,
Johns Hopkins University*

The Gaussian stochastic process (GaSP) is a useful technique for predicting nonlinear outcomes. The estimated mean function in a GaSP, however, can be far from the reality in terms of the L_2 distance. This problem was widely observed in calibrating imperfect mathematical models using experimental data, when the discrepancy function is modeled as a GaSP. In this work, we study the theoretical properties of the scaled Gaussian stochastic process (S-GaSP), a new stochastic process to address the identifiability problem of the mean function in the GaSP model. The GaSP is a special case of the S-GaSP with the scaling parameter being zero. We establish the explicit connection between the GaSP and S-GaSP through the orthogonal series representation. We show the predictive mean estimator in the S-GaSP calibration model converges to the reality at the same rate as the GaSP with the suitable choice of the regularization parameter and scaling parameter. We also show the calibrated mathematical model in the S-GaSP calibration converges to the one that minimizes the L_2 loss between the reality and mathematical model with the same regularization and scaling parameters, whereas the GaSP model does not have this property. From the regularization perspective, the loss function from the S-GaSP calibration penalizes the native norm and L_2 norm of the discrepancy function simultaneously, whereas the one from the GaSP calibration only penalizes the native norm of the discrepancy function. The predictive error from the S-GaSP matches well with the theoretical bound, and numerical evidence is presented concerning the performance of the studied approaches. Both the GaSP and S-GaSP calibration models are implemented in the “RobustCalibration” R Package on CRAN.

1. Introduction. In scientific and engineering studies, mathematical models are developed by scientists and engineers based on their expert knowledge to reproduce the physical reality. With the rapid development of the computational technique in recent years, many mathematical models are implemented in computer code, often referred as computer models or

Keywords and phrases: convergence, identifiability, orthogonal series representation, penalized kernel ridge regression, regularization, scaled Gaussian stochastic process prior

simulators.

Some parameters of the mathematical model are often unknown or unobservable in experiments. For example, the Kīlauea volcano recently has one of the biggest eruptions in history. The location and volume of the magma chamber, as well as the magma supply and storage rate of this volcano, however, is unobservable. Some field data, such as the satellite interferograms for the ground deformation and gas emission data were used to estimate these parameters for the Kīlauea volcano [1, 2, 11]. Using the field data to estimate the parameters in the mathematical model, and to identify the possible discrepancy between the mathematical model and the reality is widely known as the inverse problem or calibration [3, 4, 15, 27, 32].

Assume the field or experimental data $y^F(\mathbf{x})$ at any the observable input $\mathbf{x} \in \mathcal{X}$ can be represented as a noisy assessment of the unknown reality

$$(1.1) \quad y^F(\mathbf{x}) = y^R(\mathbf{x}) + \epsilon,$$

where $y^R(\cdot)$ is the unknown deterministic function of the reality and $\epsilon \sim N(0, \sigma_0^2)$ is a Gaussian noise with an unknown variance σ_0^2 . Denote $f^M(\mathbf{x}, \boldsymbol{\theta})$ the mathematical model at the observable inputs $\mathbf{x} \in \mathcal{X}$ and the calibration parameters $\boldsymbol{\theta} \in \boldsymbol{\Theta}$. Since the mathematical model is often imperfect to describe the physical reality, one often assumes $y^R(\mathbf{x}) = f^M(\mathbf{x}, \boldsymbol{\theta}) + \delta(\mathbf{x})$, where $\delta(\cdot)$ is a discrepancy function between the reality and mathematical model. With this specification, we have the following calibration model for an imperfect mathematical model

$$(1.2) \quad y^F(\mathbf{x}) = f^M(\mathbf{x}, \boldsymbol{\theta}) + \delta(\mathbf{x}) + \epsilon.$$

When the mean and trend of the reality is properly explained in the mathematical model, the discrepancy function is often modeled as a zero-mean Gaussian stochastic process (GaSP) [15], resulting in a closed-form expression of the predictive distribution of the reality. It was found in many following-up studies that, however, modeling the discrepancy function by a GaSP causes an identifiability problem of the calibration parameters and consequently, the calibrated mathematical model is far away from the reality (see, for example, [3, 26, 31]).

The calibration model (1.2) is also often used in modeling spatially correlated data, where $f^M(\mathbf{x}, \boldsymbol{\theta})$ is often assumed to be a parametric model for the linear fixed effect of some covariates, and $\delta(\mathbf{x})$ is a spatial random effect at the spatial coordinate \mathbf{x} . However, it is also found in many studies that the spatial random effect is confounded with the fixed effect [14, 22].

Many recent studies measure the goodness of calibration by the L_2 loss between the calibrated mathematical model and reality [26, 27, 31]. These

studies seek to find an estimator of $\boldsymbol{\theta}$ that converges to $\boldsymbol{\theta}_{L_2}$, which minimizes the L_2 distance between the reality and mathematical model, i.e.,

$$(1.3) \quad \boldsymbol{\theta}_{L_2} := \arg \min_{\boldsymbol{\theta} \in \boldsymbol{\Theta}} \int_{\mathbf{x} \in \mathcal{X}} [y^R(\mathbf{x}) - f^M(\mathbf{x}, \boldsymbol{\theta})]^2 d\mathbf{x}.$$

In [26], for instance, the reality is first estimated through a nonparametric regression model without the assistance of the mathematical model. The calibration parameters are then estimated by minimizing the L_2 loss between the calibrated mathematical model and the estimator of the reality.

On the other hand, integrating the mathematical model and discrepancy function in (1.2) for prediction is found to have a smaller predictive error than simply using a GaSP or a mathematical model alone [15]. This is because the mathematical model is developed based on the expert knowledge, which contains the information of the complex reality, and the GaSP is a flexible model for the discrepancy not captured by the calibrated mathematical model. The prediction by combining the mathematical model and discrepancy function, however, is sometimes less interpretable by scientists, as the discrepancy function can introduce some nonlinear effect that is hard to be explained. Because of the interpretation reason, one also hopes the calibrated mathematical model can predict the reality well, and this partially explains why some previous studies define $\boldsymbol{\theta}_{L_2}$ as the optimum of the calibration parameters.

To prevent the calibrated mathematical model deviating too much from the reality, we propose to model the discrepancy function by a new stochastic process, called the scaled Gaussian stochastic process (S-GaSP). The S-GaSP is first proposed in [11], where the S-GaSP is shown to be a GaSP with a transformed kernel and the computational complexity is the same as the GaSP. In this work, we provide a theoretical framework of the S-GaSP for calibration and prediction. Moreover, we also establish the connection between the maximum likelihood estimator and the kernel ridge regression estimator in the calibration setting. This connection allows us to study the asymptotic properties of the maximum likelihood estimator using some well-developed tools for the kernel ridge regression.

We highlight several advantages of using the S-GaSP to model the discrepancy function in the calibration model (1.2). First of all, we show that the predictive mean from the S-GaSP converges to the reality at the same rate as the one from the GaSP with the suitable choice of the regularization and scaling parameters. Furthermore, with the same regularization and scaling parameters, the calibration parameters in the S-GaSP can also converge to $\boldsymbol{\theta}_{L_2}$, which minimizes the L_2 distance between the reality and calibrated

mathematical model. The estimated calibration parameters in the GaSP calibration model, in contrast, do not converge to θ_{L_2} , and the predictive error by the calibrated mathematical model is large as a consequence. Thirdly, since the S-GaSP can be shown as a GaSP with a transformed kernel, the predictive distribution also has an explicit form that is easy to compute. This allows us to combine the mathematical model and discrepancy function in a coherent statistical model to both predict the reality and calibrate the mathematical model. Lastly, we found that the out-of-sample predictive error by combining the calibrated mathematical model and the discrepancy function via the S-GaSP is also slightly smaller than that using a GaSP in our numerical experiments, as the mathematical model is estimated closer to the reality in the S-GaSP.

This paper is organized as follows. In Section 2, we review the background of the GaSP and the reproducing kernel Hilbert space. The connection between the maximum likelihood estimator and the kernel ridge regression estimator is also studied. In Section 3, we introduce the S-GaSP along with the orthogonal series representation of the process and the covariance function. Two convergence issues are discussed in Section 4. We first show that the predictive mean of the reality in the S-GaSP calibration converges to the reality with the optimal rate in Section 4.1. Then we show the estimated calibration parameters also converge to θ_{L_2} in the S-GaSP calibration model in Section 4.2. In Section 5, we introduce the discretized S-GaSP along with the parameter estimation. Section 6 provides some numerical studies comparing the GaSP, the S-GaSP, and two other estimation approaches. We conclude this work in Section 7 and the proof is given in Appendices.

2. Background: Gaussian stochastic process. We first review the Gaussian stochastic process and the reproducing kernel Hilbert space in this section. Assume the mean and trend of the reality are properly modeled in the mathematical model. Consider to model the unknown discrepancy function in the calibration model (1.2) via a real-valued zero-mean Gaussian stochastic process $\delta(\cdot)$ on a p -dimensional input domain \mathcal{X} ,

$$(2.1) \quad \delta(\cdot) \sim \text{GaSP}(0, \sigma^2 K(\cdot, \cdot)),$$

where σ^2 is a variance parameter and $K(\mathbf{x}_a, \mathbf{x}_b)$ is the correlation for any $\mathbf{x}_a, \mathbf{x}_b \in \mathcal{X}$, parameterized by a kernel function. For simplicity, we assume $\mathcal{X} = [0, 1]^p$ in this work.

For any $\{\mathbf{x}_1, \dots, \mathbf{x}_n\}$, the outputs $(\delta(\mathbf{x}_1), \dots, \delta(\mathbf{x}_n))^T$ follow a multivariate normal distribution

$$(2.2) \quad [\delta(\mathbf{x}_1), \dots, \delta(\mathbf{x}_n) \mid \sigma^2, \mathbf{R}] \sim \text{MN}(\mathbf{0}, \sigma^2 \mathbf{R}),$$

where the (i, j) entry of \mathbf{R} is $K(\mathbf{x}_i, \mathbf{x}_j)$. Some frequently used kernel functions include the power exponential kernel and the Matérn kernel. We defer the issue of estimating the parameters in the kernel function in Section 5 and assume $K(\cdot, \cdot)$ is known for now.

The reproducing kernel Hilbert space (RKHS), denoted as \mathcal{H} , attached to the Gaussian stochastic process $\text{GaSP}(0, \sigma^2 K(\cdot, \cdot))$, is the completion of the space of all functions

$$\mathbf{x} \rightarrow \sum_{i=1}^k w_i K(\mathbf{x}_i, \mathbf{x}), \quad w_1, \dots, w_k \in \mathbb{R}, \mathbf{x}_1, \dots, \mathbf{x}_k, \mathbf{x} \in \mathcal{X}, k \in \mathbb{N},$$

with the inner product

$$\left\langle \sum_{i=1}^k w_i K(\mathbf{x}_i, \cdot), \sum_{j=1}^m w_j K(\mathbf{x}_j, \cdot) \right\rangle_{\mathcal{H}} = \sum_{i=1}^k \sum_{j=1}^m w_i w_j K(\mathbf{x}_i, \mathbf{x}_j).$$

For any function $f(\cdot) \in \mathcal{H}$, denote $\|f\|_{\mathcal{H}} = \sqrt{\langle f, f \rangle_{\mathcal{H}}}$ the RKHS norm or the native norm. Because the evaluation maps in RKHS are bounded linear, it follows from the Riesz representation theorem that for each $\mathbf{x} \in \mathcal{X}$ and $f(\cdot) \in \mathcal{H}$, one has $f(\mathbf{x}) = \langle f(\cdot), K(\cdot, \mathbf{x}) \rangle_{\mathcal{H}}$.

Denote $L_2(\mathcal{X})$ the space of square-integrable functions $f : \mathcal{X} \rightarrow \mathbb{R}$ with $\int_{\mathbf{x} \in \mathcal{X}} f^2(\mathbf{x}) d\mathbf{x} < \infty$. We denote $\langle f, g \rangle_{L_2(\mathcal{X})} := \int_{\mathbf{x} \in \mathcal{X}} f(\mathbf{x}) g(\mathbf{x}) d\mathbf{x}$ the usual inner product in $L_2(\mathcal{X})$. By the Mercer's theorem, there exists an orthonormal sequence of continuous eigenfunctions $\{\phi_k\}_{k=1}^{\infty}$ with a sequence of non-increasing and non-negative eigenvalues $\{\rho_k\}_{k=1}^{\infty}$ such that

$$(2.3) \quad K(\mathbf{x}_a, \mathbf{x}_b) = \sum_{k=1}^{\infty} \rho_k \phi_k(\mathbf{x}_a) \phi_k(\mathbf{x}_b),$$

for any $\mathbf{x}_a, \mathbf{x}_b \in \mathcal{X}$.

The RKHS \mathcal{H} contains all functions $f(\cdot) = \sum_{k=1}^{\infty} f_k \phi_k(\cdot) \in L_2(\mathcal{X})$ with $f_k = \langle f, \phi_k \rangle_{L_2(\mathcal{X})}$ and $\sum_{k=1}^{\infty} f_k^2 / \rho_k < \infty$. For any $g(\cdot) = \sum_{k=1}^{\infty} g_k \phi_k(\cdot) \in \mathcal{H}$ and $f(\cdot)$, the inner product can be represented as $\langle f, g \rangle_{\mathcal{H}} = \sum_{k=1}^{\infty} f_k g_k / \rho_k$. For more properties of the RKHS, we refer to Chapter 1 of [30] and Chapter 11 of [7].

2.1. The equivalence between the maximum likelihood estimator and the kernel ridge regression estimator in calibration. Assume one has a set of observations $\mathbf{y}^F := (y^F(\mathbf{x}_1), \dots, y^F(\mathbf{x}_n))^T$ and mathematical model outputs $\mathbf{f}_{\boldsymbol{\theta}}^M := (f^M(\mathbf{x}_1, \boldsymbol{\theta}), \dots, f^M(\mathbf{x}_n, \boldsymbol{\theta}))^T$, where $\boldsymbol{\theta} = (\theta_1, \dots, \theta_q)^T \in \boldsymbol{\Theta} \subset \mathbb{R}^q$ is a q -dimensional vector of the calibration parameters.

Denote the regularization parameter $\lambda := \sigma_0^2/(n\sigma^2)$. For the calibration model (1.2) with δ modeled as a GaSP in (2.1), the marginal distribution of \mathbf{y}^F follows a multivariate normal after marginalizing out δ

$$(2.4) \quad [\mathbf{y}^F \mid \boldsymbol{\theta}, \sigma_0^2, \lambda] \sim \text{MN}(\mathbf{f}_{\boldsymbol{\theta}}^M, \sigma_0^2((n\lambda)^{-1}\mathbf{R} + \mathbf{I}_n)).$$

Let $\mathcal{L}(\boldsymbol{\theta})$ be the likelihood for $\boldsymbol{\theta}$ in (2.4) given the other parameters in the model. For any given λ , the maximum likelihood estimator (MLE) of $\boldsymbol{\theta}$ is denoted as

$$(2.5) \quad \hat{\boldsymbol{\theta}}_{\lambda,n} := \arg \max_{\boldsymbol{\theta} \in \Theta} \mathcal{L}(\boldsymbol{\theta}).$$

Conditioning on the observations, $\hat{\boldsymbol{\theta}}_{\lambda,n}$ and λ , the predictive mean of the discrepancy function at any $\mathbf{x} \in \mathcal{X}$ has the following expression

$$(2.6) \quad \hat{\delta}_{\lambda,n}(\mathbf{x}) := \mathbb{E}[\delta(\mathbf{x}) \mid \mathbf{y}^F, \hat{\boldsymbol{\theta}}_{\lambda,n}, \lambda] = \mathbf{r}^T(\mathbf{x})(\mathbf{R} + n\lambda\mathbf{I}_n)^{-1} (\mathbf{y}^F - \mathbf{f}_{\hat{\boldsymbol{\theta}}_{\lambda,n}}^M)$$

with $\mathbf{r}(\mathbf{x}) = (K(\mathbf{x}_1, \mathbf{x}), \dots, K(\mathbf{x}_n, \mathbf{x}))^T$ and \mathbf{I}_n being the n -dimensional identity matrix.

It is well-known that the predictive mean in (2.6) can be written as the estimator for the kernel ridge regression (KRR). In the following lemma, we show that $(\hat{\boldsymbol{\theta}}_{\lambda,n}, \hat{\delta}_{\lambda,n}(\cdot))$ is equivalent to the KRR estimator.

LEMMA 2.1. *The maximum likelihood estimator $\hat{\boldsymbol{\theta}}_{\lambda,n}$ defined in (2.5) and predictive mean estimator $\hat{\delta}_{\lambda,n}(\cdot)$ defined in (2.6) can be expressed as the estimator of the kernel ridge regression as follows*

$$(\hat{\boldsymbol{\theta}}_{\lambda,n}, \hat{\delta}_{\lambda,n}(\cdot)) = \arg \min_{\boldsymbol{\theta} \in \Theta, \delta(\cdot) \in \mathcal{H}} \ell_{\lambda,n}(\boldsymbol{\theta}, \delta),$$

where

$$(2.7) \quad \ell_{\lambda,n}(\boldsymbol{\theta}, \delta) = \frac{1}{n} \sum_{i=1}^n (y^F(\mathbf{x}_i) - f^M(\mathbf{x}_i, \boldsymbol{\theta}) - \delta(\mathbf{x}_i))^2 + \lambda \|\delta\|_{\mathcal{H}}^2.$$

Although modeling the discrepancy function by the GaSP typically improves the prediction accuracy of the reality, the penalty term of (2.7) only contains $\|\delta\|_{\mathcal{H}}$ to control the complexity of the discrepancy. As the RKHS norm is not equivalent to the L_2 norm, the calibrated computer model could deviate a lot from the best performed mathematical model in terms of the L_2 loss [26]. In Section 3, we introduce the scaled Gaussian stochastic process that predicts the reality as accurately as the GaSP with the aid of the mathematical model, but has more prior mass on the small L_2 distance between the reality and mathematical model. As a consequence, the KRR estimator of the new model penalizes both $\|\delta\|_{\mathcal{H}}$ and $\|\delta\|_{L_2(\mathcal{X})}$ simultaneously.

3. The scaled Gaussian stochastic process. The L_2 loss between the reality and mathematical model can be expressed as a random loss function of the discrepancy function $Z := \int_{\mathbf{x} \in \mathcal{X}} (y^R(\mathbf{x}) - f^M(\mathbf{x}, \boldsymbol{\theta}))^2 d\mathbf{x} = \int_{\mathbf{x} \in \mathcal{X}} \delta^2(\mathbf{x}) d\mathbf{x}$. We hierarchically model the crucial random variable Z to have more probability mass near zero. The scaled Gaussian stochastic process calibration model is defined as follows

$$\begin{aligned}
 (3.1) \quad & y^F(\mathbf{x}) = f^M(\mathbf{x}, \boldsymbol{\theta}) + \delta_z(\mathbf{x}) + \epsilon, \\
 & \delta_z(\mathbf{x}) = \left\{ \delta(\mathbf{x}) \mid \int_{\boldsymbol{\xi} \in \mathcal{X}} \delta^2(\boldsymbol{\xi}) d\boldsymbol{\xi} = Z \right\}, \\
 & \delta(\cdot) \sim \text{GaSP}(0, \sigma^2 K(\cdot, \cdot)), \\
 & Z \sim p_Z(\cdot), \quad \epsilon \sim \text{N}(0, \sigma_0^2).
 \end{aligned}$$

We call $\delta_z(\cdot)$ the scaled Gaussian stochastic process (S-GaSP). Given $Z = z$, the S-GaSP becomes the GaSP constrained at the space $\int_{\mathbf{x} \in \mathcal{X}} \delta^2(\mathbf{x}) d\mathbf{x} = z$.

By definition, $Z = \int_{\mathbf{x} \in \mathcal{X}} \delta^2(\mathbf{x}) d\mathbf{x}$. Conditioning on all parameters in the model, a simple choice of $p_Z(\cdot)$ is

$$(3.2) \quad p_Z(z) = \frac{g_Z(z) p_\delta(Z = z)}{\int_0^\infty g_Z(t) p_\delta(Z = t) dt},$$

where $g_Z(z)$ is a non-increasing scaling function and $p_\delta(Z = z)$ is the density of Z at z induced by the GaSP in (2.1). The measure for Z induced by the S-GaSP is proportional to the measure of Z induced by the GaSP scaled by a non-increasing scaling function $g_Z(z)$ to have more probability mass near zero than the unconstrained GaSP does.

When $g_Z(\cdot)$ is a constant function, the S-GaSP becomes the GaSP without the constraint. Following [11], conditioning on all parameters, we assume

$$(3.3) \quad g_Z(z) = \frac{\lambda_z}{2\sigma^2} \exp\left(-\frac{\lambda_z z}{2\sigma^2}\right),$$

where λ_z is a non-negative scaling parameter.

The benefit of using $p_Z(\cdot)$ in (3.2) and $g_Z(\cdot)$ in (3.3) is that any marginal distribution of δ_z still follows a multivariate normal distribution (see Lemma 2.3 in [11]). In Section 3.1, we explore the orthogonal series representation of the S-GaSP.

3.1. Orthogonal series representation. Based on Karhunen-Loève theorem, a GaSP admits the following representation for any $\mathbf{x} \in \mathcal{X}$

$$(3.4) \quad \delta(\mathbf{x}) = \sigma \sum_{k=1}^{\infty} \sqrt{\rho_k} Z_k \phi_k(\mathbf{x}),$$

where $Z_k \stackrel{i.i.d.}{\sim} N(0, 1)$, ρ_k and $\phi_k(\cdot)$ are the k th eigenvalue and eigenfunction of the kernel $K(\cdot, \cdot)$, respectively.

The following lemma shows that the S-GaSP can also be represented as an orthogonal random series with independent normal coefficients.

LEMMA 3.1 (Karhunen-Loève expansion for the S-GaSP). *Assume $p_Z(\cdot)$ and $g_Z(\cdot)$ are defined in (3.2) and (3.3), respectively. For any $\mathbf{x} \in \mathcal{X}$, the S-GaSP defined in (3.1) has the following representation*

$$\delta_z(\mathbf{x}) = \sigma \sum_{k=1}^{\infty} \sqrt{\frac{\rho_k}{1 + \lambda_z \rho_k}} Z_k \phi_k(\mathbf{x}),$$

where $Z_k \stackrel{i.i.d.}{\sim} N(0, 1)$, ρ_k and $\phi_k(\cdot)$ are the k th eigenvalue and eigenfunction of the kernel $K(\cdot, \cdot)$, respectively.

The covariance function of the S-GaSP can also be decomposed as an infinite orthogonal series, which is an immediate consequence of the fact that the S-GaSP is indeed a GaSP with a transformed kernel (see Lemma 2.3 in [11]) and Lemma 3.1.

COROLLARY 3.1. *Assume $p_Z(\cdot)$ and $g_Z(\cdot)$ are defined in (3.2) and (3.3), respectively. The marginal distribution of the S-GaSP defined in (3.1) follows a multivariate normal distribution*

$$[\delta_z(\mathbf{x}_1), \dots, \delta_z(\mathbf{x}_n) \mid \sigma^2 \mathbf{R}_z] \sim MN(\mathbf{0}, \sigma^2 \mathbf{R}_z),$$

where the (i, j) entry of \mathbf{R}_z is

$$(3.5) \quad K_z(\mathbf{x}_i, \mathbf{x}_j) = \sum_{k=1}^{\infty} \frac{\rho_k}{1 + \lambda_z \rho_k} \phi(\mathbf{x}_i) \phi(\mathbf{x}_j).$$

Corollary 3.1 implies that the i th eigenvalue of the kernel function $K_z(\cdot, \cdot)$ in the S-GaSP is $\rho_{z,k} := \rho_k / (1 + \lambda_z \rho_k)$ and the k th eigenfunction $\phi_k(\cdot)$ is the same as the one in the GaSP. The form (3.5) does not give an explicit expression for the kernel in the S-GaSP. Instead of truncating the series, one can discretize the integral $\int_{\xi \in \mathcal{X}} \delta(\xi)^2 d\xi$ at finitely many constraint points. This discretizing procedure leads to an explicit expression of the covariance matrix in the likelihood, discussed in Section 5.

It is shown in [11] that the random L_2 loss induced by the GaSP can be written as an infinite weighted sum of independent chi-squared random variables. The following corollary provides a similar decomposition of Z in the S-GaSP, which follows from Lemma 2.1 in [11] and Corollary 3.1.

COROLLARY 3.2. *Assume the same conditions in Lemma 3.1 hold. The distribution of $Z = \int_{\mathbf{x} \in \mathcal{X}} \delta^2(\mathbf{x}) d\mathbf{x}$ induced by the S-GaSP follows*

$$Z \sim \sigma^2 \sum_{k=1}^{\infty} \frac{\rho_k}{1 + \lambda_z \rho_k} \chi_k^2(1),$$

where $\{\chi_k^2(1)\}_{k=1}^{\infty}$ are independent chi-squared random variables with one degree of freedom.

Denote \mathcal{H} and \mathcal{H}_z the RKHS attached to GaSP with kernel $K(\cdot, \cdot)$ and the S-GaSP with kernel $K_z(\cdot, \cdot)$, respectively. We conclude this subsection by the explicit connection between the inner product of the GaSP and that of the S-GaSP.

LEMMA 3.2. *Assume $p_Z(\cdot)$ and $g_Z(\cdot)$ are defined in (3.2) and (3.3), respectively. Let $h(\cdot) = \sum_{i=1}^{\infty} h_i \phi_i(\cdot)$ and $g(\cdot) = \sum_{i=1}^{\infty} g_i \phi_i(\cdot)$ be the elements in \mathcal{H} . It holds that*

$$\langle h, g \rangle_{\mathcal{H}_z} = \langle h, g \rangle_{\mathcal{H}} + \lambda_z \langle h, g \rangle_{L_2(\mathcal{X})}.$$

3.2. Estimation for the S-GaSP. With the specification of the density $p_Z(\cdot)$ and scaling function $g_Z(\cdot)$ for the distribution of Z in (3.2) and (3.3), respectively, after marginalizing out δ_z in (3.1), the marginal likelihood for θ in the S-GaSP follows a multivariate normal distribution

$$(3.6) \quad [\mathbf{y}^F \mid \theta, \sigma_0^2, \lambda, \lambda_z] \sim \text{MN}(\mathbf{f}_{\theta}^M, \sigma_0^2((n\lambda)^{-1}\mathbf{R}_z + \mathbf{I}_n)).$$

Denote $\mathcal{L}_z(\theta)$ the likelihood for θ in (3.6). Similarly, we have the equivalence between the MLE and the KRR estimator for the S-GaSP calibration, where both the RKHS norm and L_2 norm of the discrepancy function are penalized in the loss function, stated in Lemma 3.3 below.

LEMMA 3.3. *The maximum likelihood estimator $\hat{\theta}_{\lambda, \lambda_z, n} := \arg \max_{\theta \in \Theta} \mathcal{L}_z(\theta)$ and predictive mean $\hat{\delta}_{\lambda, \lambda_z, n}(\cdot) := \mathbb{E}[\delta_z(\cdot) \mid \mathbf{y}^F, \hat{\theta}_{\lambda, \lambda_z, n}, \lambda, \lambda_z]$ are the same as the estimator of the penalized kernel ridge regression*

$$(\hat{\theta}_{\lambda, \lambda_z, n}, \hat{\delta}_{\lambda, \lambda_z, n}(\cdot)) = \arg \min_{\delta(\cdot) \in \mathcal{H}, \theta \in \Theta} \ell_{\lambda, \lambda_z, n}(\theta, \delta),$$

where

$$(3.7) \quad \ell_{\lambda, \lambda_z, n}(\theta, \delta) = \frac{1}{n} \sum_{i=1}^n (y^F(\mathbf{x}_i) - f^M(\mathbf{x}_i, \theta) - \delta(\mathbf{x}_i))^2 + \lambda \|\delta\|_{\mathcal{H}_z}^2,$$

with $\|\delta\|_{\mathcal{H}_z}^2 = \|\delta\|_{\mathcal{H}}^2 + \lambda_z \|\delta\|_{L_2(\mathcal{X})}^2$.

4. Convergence properties.

4.1. *Nonparametric regression by the S-GaSP.* Let us first consider the following nonparametric regression model,

$$(4.1) \quad y(\mathbf{x}_i) = f(\mathbf{x}_i) + \epsilon_i, \quad \epsilon_i \stackrel{i.i.d.}{\sim} N(0, \sigma_0^2), \quad i = 1, \dots, n,$$

where f is assumed to follow the zero-mean S-GaSP prior with the default choice of $p_Z(\cdot)$ and $g_Z(\cdot)$ in (3.2) and (3.3), respectively. For simplicity, we assume that $\mathbf{x}_1, \dots, \mathbf{x}_n$ are independently sampled from $\text{Unif}([0, 1]^p)$.

Assume the underlying truth $f_0(\cdot) := E_y[y(\cdot)]$ resides in the p -dimensional Sobolev space $\mathcal{W}_2^m(\mathcal{X})$ with $m > p/2$, where

$$(4.2) \quad \mathcal{W}_2^m(\mathcal{X}) = \left\{ f(\cdot) = \sum_{k=1}^{\infty} f_k \phi_k(\cdot) \in L_2(\mathcal{X}) : \sum_{k=1}^{\infty} k^{2m/p} f_k^2 < \infty \right\},$$

with $\{\phi_k(\cdot)\}_{k=1}^{\infty}$ being a sequence of the orthonormal basis of $L_2(\mathcal{X})$. For any integer vector $\mathbf{k} = (k_1, \dots, k_p)^T$ and a function $f(x_1, \dots, x_p) : \mathcal{X} \rightarrow \mathbb{R}$, denote $D^{\mathbf{k}}$ the mixed partial derivative operator $D^{\mathbf{k}}f(\cdot) := \partial^{|\mathbf{k}|} f(\cdot) / \partial^{k_1} x_1 \dots \partial^{k_p} x_p$ with $|\mathbf{k}| = \sum_{i=1}^p k_i$. For any function in $\mathcal{W}_2^m(\mathcal{X})$, we have $\|D^{\mathbf{k}}f(\cdot)\|_{L_2(\mathcal{X})} < \infty$ for any $|\mathbf{k}| < m$.

Recall that $\lambda = \sigma_0^2/(n\sigma^2)$. The posterior mean estimator of the S-GaSP is equivalent to the KRR estimator as follows

$$(4.3) \quad \hat{f}_{\lambda, \lambda_z, n} = \arg \min_{f \in \mathcal{H}} \left[\frac{1}{n} \sum_{i=1}^n (y(\mathbf{x}_i) - f(\mathbf{x}_i))^2 + \lambda \|f\|_{\mathcal{H}}^2 + \lambda \lambda_z \|f\|_{L_2(\mathcal{X})}^2 \right].$$

Recall $\{\rho_k\}_{k=1}^{\infty}$ and $\{\phi_k\}_{k=1}^{\infty}$ are the sequence of the eigenvalues and eigenfunctions of the reproducing kernel $K(\cdot, \cdot)$ associated with \mathcal{H} , respectively. For all k , we assume the eigenvalues satisfy

$$(4.4) \quad c_\rho k^{-2m/p} \leq \rho_k \leq C_\rho k^{-2m/p},$$

for some constants c_ρ and $C_\rho > 0$. For all $k \in \mathbb{N}^+$ and $\mathbf{x} \in \mathcal{X}$, we assume the eigenfunctions are bounded uniformly,

$$(4.5) \quad \sup_{\mathbf{x} \in \mathcal{X}} |\phi_k(\mathbf{x})| \leq C_\phi,$$

where $C_\phi > 0$ is a constant depending on the kernel $K(\cdot, \cdot)$.

As a motivating example, the Matérn kernel satisfies the decay rate of the eigenvalues in (4.4) when expanded with respect to the Fourier basis [35].

The exact form of the Matérn kernel along with the parameterization and parameter estimation is discussed in Section 5.1.

We are now ready to state the convergence rate of the S-GaSP for the nonparametric regression model in (4.1).

THEOREM 4.1. *Assume the eigenvalues and eigenfunctions of $K(\cdot, \cdot)$ satisfy (4.4) and (4.5), respectively. Further assume $f_0 \in \mathcal{W}_2^m(\mathcal{X})$ and denote $\beta := (2m-p)^2/\{2m(2m+p)\}$. Consider the nonparametric regression model (4.1). For sufficiently large n , any $\alpha > 2$ and $C_\beta \in (0, 1)$, with probability at least $1 - \exp\{-(\alpha - 2)/3\} - \exp(-n^{C_\beta\beta})$,*

$$\|\hat{f}_{\lambda, \lambda_z, n} - f_0\|_{L_2(\mathcal{X})} \leq 2 \left[\sqrt{2} (\|f_0\|_{L_2(\mathcal{X})} + \|f_0\|_{\mathcal{H}}) + C_K \sigma_0 \sqrt{\alpha} \right] n^{-\frac{m}{2m+p}}$$

and

$$\|\hat{f}_{\lambda, \lambda_z, n} - f_0\|_{\mathcal{H}} \leq 2 \left[\sqrt{2} (\|f_0\|_{L_2(\mathcal{X})} + \|f_0\|_{\mathcal{H}}) + C_K \sigma_0 \sqrt{\alpha} \right]$$

by choosing $\lambda = n^{-2m/(2m+p)}$ and $\lambda_z = \lambda^{-1/2}$, where C_K is a constant only depending on the kernel $K(\cdot, \cdot)$.

The conditions in Theorem 4.1 can be relaxed in various ways. From the proof of Theorem 4.1, it is easy to see that if $\lambda = O(n^{-2m/(2m+p)})$ and $\lambda_z \leq O(\lambda^{-1/2})$, the estimator still converges to the reality in L_2 distance with the same rate $O(n^{-m/(2m+p)})$. In practice, a small λ often leads to a small predictive error [30]. The estimation of λ and the parameters in the kernel function are discussed in Section 5.1. Furthermore, although the stationarity of the process is often assumed for the computational purpose, it is not required in Theorem 4.1.

The estimator for the reality in the S-GaSP calibration model is defined as follows

$$\hat{y}_{\lambda, \lambda_z, n}^R(\mathbf{x}) := f^M(\mathbf{x}, \hat{\boldsymbol{\theta}}_{\lambda, \lambda_z, n}) + \hat{\delta}_{\lambda, \lambda_z, n}(\mathbf{x})$$

for any $\mathbf{x} \in \mathcal{X}$, where $(\hat{\boldsymbol{\theta}}_{\lambda, \lambda_z, n}, \hat{\delta}_{\lambda, \lambda_z, n})$ is the estimator of the penalized KRR obtained by minimizing the loss in (3.7). The following Corollary 4.1 gives the convergence rate of the S-GaSP calibration model in predicting the reality.

COROLLARY 4.1. *Assume $y^R(\cdot) - f^M(\cdot, \boldsymbol{\theta}) \in \mathcal{W}_2^m(\mathcal{X})$ for any $\boldsymbol{\theta} \in \boldsymbol{\Theta}$ and $\sup_{\boldsymbol{\theta} \in \boldsymbol{\Theta}} \|y^R(\cdot) - f^M(\cdot, \boldsymbol{\theta})\|_{\mathcal{H}} < \infty$. Let the eigenvalues and eigenfunctions of $K(\cdot, \cdot)$ satisfy (4.4) and (4.5), respectively. For sufficiently large n and any*

$\alpha > 2$ and $C_\beta \in (0, 1)$, with probability at least $1 - \exp\{-(\alpha - 2)/3\} - \exp(-n^{C_\beta\beta})$,

$$\begin{aligned} \|\hat{y}_{\lambda, \lambda_z, n}^R(\cdot) - y^R(\cdot)\|_{L_2(\mathcal{X})} &\leq 2 \left[\sqrt{2} \left(\sup_{\boldsymbol{\theta} \in \boldsymbol{\Theta}} \|y^R(\cdot) - f^M(\cdot, \boldsymbol{\theta})\|_{L_2(\mathcal{X})} \right. \right. \\ &\quad \left. \left. + \sup_{\boldsymbol{\theta} \in \boldsymbol{\Theta}} \|y^R(\cdot) - f^M(\cdot, \boldsymbol{\theta})\|_{\mathcal{H}} \right) + C_K \sigma_0 \sqrt{\alpha} \right] n^{-\frac{m}{2m+p}} \end{aligned}$$

by choosing $\lambda = n^{-2m/(2m+p)}$ and $\lambda_z = \lambda^{-1/2}$, where C_K is a constant only depending on the kernel $K(\cdot, \cdot)$ and $\beta = (2m - p)^2/(2m(2m + p))$.

The conditions can be relaxed by choosing $\lambda = O(n^{-2m/(2m+p)})$ and $\lambda_z \leq O(\lambda^{-1/2})$ to obtain the same convergence rate.

We illustrate the convergence using the following example, where $y^R(\cdot)$ lies in the Sobolev space $\mathcal{W}_2^m(\mathcal{X})$ with $m = 3$ and $\mathcal{X} = [0, 1]$ [34].

EXAMPLE 4.1. Let the reality be $y^R(x) = 2 \sum_{j=1}^{\infty} j^{-3} \cos(\pi(j-0.5)x) \sin(j)$, and consider $y^F(x) = y^R(x) + \epsilon$, where $\epsilon \sim N(0, 0.05^2)$ is a Gaussian noise. Let the mathematical model be a mean parameter, i.e. $f^M(x, \theta) = \theta$. The goal is to predict $y^R(x)$ at $x \in [0, 1]$ and estimate θ .

Assume $K(\cdot, \cdot)$ follows the Matérn kernel in (5.5) with the range parameter $\gamma = 1$. The eigenvalues of this kernel satisfy (4.4) with $m = 3$. We test 50 configurations with the number of observations $n \in [\exp(5), \exp(10)]$, and the design points $\{x_i\}_{i=1}^n$ are equally spaced in $[0, 1]$. In each configuration, $N = 100$ simulation replicates are implemented. We perform predictions on $n^* = 3 \times 10^4$ inputs equally spaced from $[0, 1]$ using the average root of the mean squared error (AvgRMSE) to validate as follows

$$(4.6) \quad \text{AvgRMSE}_{f^M+\delta} = \frac{1}{N} \sum_{i=1}^N \sqrt{\frac{1}{n^*} \sum_{j=1}^{n^*} (\hat{y}_i^R(\mathbf{x}_j^*) - y_i^R(\mathbf{x}_j^*))^2},$$

where $\hat{y}_i^R(\mathbf{x}_j^*)$ is an estimator of the reality at \mathbf{x}_j^* for $j = 1, \dots, n^*$. The subscript $f^M + \delta$ means both the calibrated mathematical model and discrepancy function are used for prediction.

Figure 1 presents the predictive error of the GaSP calibration and the S-GaSP calibration for Example 4.1. In the left panel, the red circles are the $\text{AvgRMSE}_{f^M+\delta}$ using the predictive mean of the calibration model in (1.2) with δ modeled as a GaSP in (2.1), and the blue circles are $\text{AvgRMSE}_{f^M+\delta}$ using the predictive mean of the discretized S-GaSP calibration in (5.1)

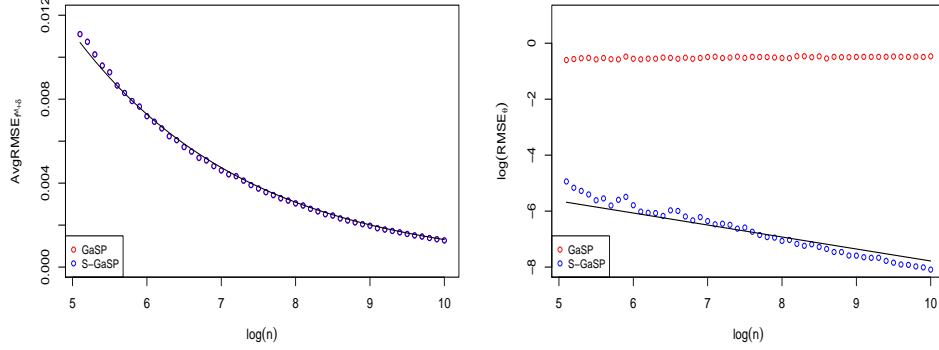


FIG 1. Calibration and prediction by the GaSP and discretized S-GaSP calibration models for Example 4.1. In the left panel, the $\text{AvgRMSE}_{f^{M+\delta}}$ of the GaSP calibration and that of the discretized S-GaSP calibration are graphed as the red and blue circles, respectively; the black curve is $n^{-m/(2m+p)}/10.5$, representing the theoretical upper bound by Corollary 4.1 (up to a constant). In the right panel, the natural logarithm of the RMSE_{θ} of the GaSP calibration and that of the discretized S-GaSP calibration is graphed as the red circles and blue circles, respectively; the black line is $\log(n^{-m/(2m+p)}/33)$, representing the theoretical upper bound from Theorem 4.2 (up to a constant). $\lambda = n^{-2m/(2m+p)} \times 10^{-4}$ with $m = 3$, $p = 1$ and $\lambda_z = \lambda^{-1/2}$ are assumed. The red and blue circles overlap in the left panel.

discussed in Section 5. The basic idea of the discretized S-GaSP is to replace the integral $\int_{\mathbf{x} \in \mathcal{X}} \delta^2(\mathbf{x}) d\mathbf{x}$ in the S-GaSP model in (3.1) by $(1/n) \sum_{i=1}^n \delta^2(\mathbf{x}_i)$ for the computational purpose. Interestingly, the red circles and blue circles overlap in the left panel and they both match perfectly well with the black curve, representing the theoretical bound from Corollary 4.1.

Since the mathematical model for Example 4.1 is only a mean parameter, the L_2 distance between the reality and the mathematical model is unimodal. We thus use the root of the mean squared error between the estimator of the calibration parameters and the L_2 minimizer θ_{L_2} as the measurement of how well the calibrated mathematical model predicts the reality as follows

$$(4.7) \quad \text{RMSE}_{\theta} = \sqrt{\frac{1}{N} \sum_{i=1}^N (\hat{\theta}_i - \theta_{L_2})^2},$$

where $\hat{\theta}_i$ is the estimator of θ in the i th experiment.

Although the GaSP and the S-GaSP perform equally well in prediction for Example 4.1, the estimator of the calibration parameter in the discretized S-GaSP calibration converges to the L_2 minimizer, but that in the GaSP

calibration does not converge to θ_{L_2} , shown in the right panel of Figure 1. This problem is caused by the difference between the RKHS norm and the L_2 norm. As illustrated in Lemma 2.1 and Lemma 3.3, both the RKHS norm and L_2 norm of the discrepancy function are penalized in the S-GaSP calibration model, whereas the GaSP calibration model only penalizes the RKHS norm of the discrepancy function.

In the Section 4.2, we further show that under some regularity conditions, the calibrated parameters in the S-GaSP calibration converges to the L_2 minimizer with the same choice of the regularization parameter and scaling parameter.

4.2. Towards reconciling the L_2 norm and RKHS norm in calibration.

We first list some regularity conditions for the convergence of calibration parameters in the S-GaSP calibration model.

A1 θ_{L_2} is the unique solution of (1.3) and it is an interior point of Θ .

A2 The Hessian matrix

$$\int \frac{\partial^2 (y^R(\mathbf{x}) - f^M(\mathbf{x}, \theta))^2}{\partial \theta \partial \theta^T} d\mathbf{x}$$

is invertible in a neighborhood of θ_{L_2} .

A3 For all $j = 1, \dots, q$, it holds that

$$\sup_{\theta \in \Theta} \left\| \frac{\partial f^M(\cdot, \theta)}{\partial \theta_j} \right\|_{\mathcal{H}} < \infty.$$

A4 The function class $\{y^R(\cdot) - f^M(\cdot, \theta) : \theta \in \Theta\}$ is Donsker.

A5 $\sup_{\theta \in \Theta} \|y^R(\cdot) - f^M(\cdot, \theta)\|_{\mathcal{H}} < \infty$.

A6 The eigenvalues and eigenfunctions of $K(\cdot, \cdot)$ satisfy (4.4) and (4.5), respectively.

Assumptions A1 to A3 are regularity conditions of θ_{L_2} and the mathematical model $y^M(\cdot, \theta)$ around θ_{L_2} . Assumptions A4 to A6 guarantee the KRR estimator $\hat{\delta}_{z, \theta}$ converges to $y^R(\cdot) - f^M(\cdot, \theta)$ uniformly for each $\theta \in \Theta$ in terms of the L_2 loss.

THEOREM 4.2. *Under assumptions A1 to A6, for the estimated calibration parameters in (3.7), one has*

$$\hat{\theta}_{\lambda, \lambda_z, n} = \theta_{L_2} + O_p(n^{-\frac{m}{2m+p}}),$$

by choosing $\lambda = O(n^{-2m/(2m+p)})$ and $\lambda_z = O(\lambda^{-1/2})$.

Note that $\lambda = O(n^{-2m/(2m+p)})$ and $\lambda_z = O(\lambda^{-1/2})$ also guarantee the predictive mean estimator in the S-GaSP calibration converges to the reality at the rate $O(n^{-m/(2m+p)})$ in terms of the L_2 loss by Corollary 4.1 and Theorem 4.2. On the contrary, the calibrated parameters of the GaSP calibration typically do not converge to the L_2 minimizer. Let $\frac{\partial f^M(\cdot, \hat{\theta})}{\partial \theta_j} := \frac{\partial f^M(\cdot, \theta)}{\partial \theta_j} \big|_{\theta = \hat{\theta}}$. A key difference between the GaSP and the S-GaSP calibration is stated in the following Corollary 4.2, which is an immediate consequence from the proof of Theorem 4.2.

COROLLARY 4.2. *Under assumptions A1 to A6, the estimator for the calibration parameters in the S-GaSP calibration in (3.7) satisfies*

$$\frac{1}{\lambda_z} \left\langle \hat{\delta}_{\lambda, \lambda_z, n}(\cdot), \frac{\partial f^M(\cdot, \hat{\theta}_{\lambda, \lambda_z, n})}{\partial \theta_j} \right\rangle_{\mathcal{H}} + \left\langle \hat{\delta}_{\lambda, \lambda_z, n}(\cdot), \frac{\partial f^M(\cdot, \hat{\theta}_{\lambda, \lambda_z, n})}{\partial \theta_j} \right\rangle_{L_2(\mathcal{X})} = 0;$$

Further assuming the mathematical model is differentiable at $\hat{\theta}_{\lambda, n}$ in (2.7), the estimator of the calibration parameters in the GaSP calibration satisfies

$$\left\langle \hat{\delta}_{\lambda, n}(\cdot), \frac{\partial f^M(\cdot, \hat{\theta}_{\lambda, n})}{\partial \theta_j} \right\rangle_{\mathcal{H}} = 0,$$

for any θ_j , $j = 1, \dots, q$.

To ensure the convergence of an estimator $\hat{\theta}$ to the L_2 minimizer, one typical requirement is that $\langle \hat{\delta}_{L_2}(\cdot), \frac{\partial f^M(\cdot, \hat{\theta})}{\partial \theta_j} \rangle_{L_2(\mathcal{X})} = o_p(1)$. It is easy to see that the S-GaSP satisfies this condition with $1/\lambda_z = o(1)$. However, because of the difference between the RKHS norm and L_2 norm, the estimated parameters $\hat{\theta}_{\lambda, n}$ in the GaSP calibration model can be far away from the L_2 minimizer. As a result, the calibrated mathematical model may not predict the reality accurately in the GaSP calibration model, as found in many previous studies [3, 11, 26, 31].

Theorem 4.2 states that the convergence rate of θ in the S-GaSP calibration (to θ_{L_2}) is slightly slower than $O(n^{-1/2})$ by choosing $\lambda = O(n^{-2m/(2m+p)})$ and $\lambda_z = O(\lambda^{-1/2})$. The $O(n^{-1/2})$ convergence rate of the calibration parameters can be obtained by choosing a larger λ_z along with the increase of the number of observations, but the convergence rate to the reality obtained in (4.1) may decrease. The slower convergence rate to θ_{L_2} in the S-GaSP reflects the added uncertainty of the parameter estimation caused by the model discrepancy. A numerical example will be given in Section 6 to illustrate the difference between the GaSP, the S-GaSP calibration and other approaches seeking to find the L_2 minimizer θ_{L_2} .

We graph the natural logarithm of RMSE_θ for Example 4.1 in the GaSP and the discretized S-GaSP calibration as the red circles and blue circles in the right panel of Figure 1, respectively. The estimated parameters in the discretized S-GaSP calibration converges to the L_2 minimizer when the sample size goes large, whereas the GaSP calibration does not. The convergence of $\hat{\theta}_{\lambda, \lambda_z, n}$ to the L_2 minimizer may look faster in Figure 1 compared with the theoretical upper bound shown in Theorem 4.2. This is because λ_z is chosen to be large, resulting in $\langle \hat{\delta}_{L_2}(\cdot), \frac{\partial f^M(\cdot, \hat{\theta}_{\lambda, \lambda_z, n})}{\partial \theta_j} \rangle_{L_2(\mathcal{X})} \approx 0$, in which case the S-GaSP behaves similarly to some other approaches that estimate the calibration parameters by minimizing the L_2 loss for this example [26, 31].

5. Discretized scaled Gaussian stochastic process. We address the computational issue in the S-GaSP calibration in this section. Instead of truncating the kernel function in (3.5) by the first several terms, following the approach in [11], one can select N_C distinct points to discretize the input space $[0, 1]^p$ and replace $\int_{\xi \in \mathcal{X}} \delta(\xi)^2 d\xi$ by $(1/N_C) \sum_{i=1}^{N_C} \delta(\mathbf{x}_i^C)^2$ in the S-GaSP model in (3.1).

Here we let the discretization points be the observed inputs, i.e. $\mathbf{x}_i^C = \mathbf{x}_i$ for $i = 1, \dots, N_C$ and $N_C = n$. The discretized S-GaSP is then defined as

$$\begin{aligned}
 (5.1) \quad & y^F(\mathbf{x}) = f^M(\mathbf{x}, \boldsymbol{\theta}) + \delta_{z_d}(\mathbf{x}) + \epsilon, \\
 & \delta_{z_d}(\mathbf{x}) = \left\{ \delta(\mathbf{x}) \mid \frac{1}{n} \sum_{i=1}^n \delta(\mathbf{x}_i)^2 = Z_d \right\} \\
 & \delta(\cdot) \sim \text{GaSP}(0, \sigma^2 K(\cdot, \cdot)), \\
 & Z_d \sim p_{Z_d}(\cdot), \epsilon \sim N(0, \sigma_0^2).
 \end{aligned}$$

Assume $\delta_{z_d}(\cdot)$ is defined in (5.1) with $p_{Z_d}(\cdot)$ and $g_{Z_d}(\cdot)$ defined in (3.2) and (3.3), respectively. After marginalizing out Z , it follows from Lemma 2.4 in [11] that $\delta_{z_d}(\cdot)$ is still a zero-mean GaSP with the covariance function

$$(5.2) \quad \sigma^2 K_{z_d}(\mathbf{x}_a, \mathbf{x}_b) = \sigma^2 (K(\mathbf{x}_a, \mathbf{x}_b) - \mathbf{r}^T(\mathbf{x}_a) \tilde{\mathbf{R}}^{-1} \mathbf{r}(\mathbf{x}_b))$$

for any $\mathbf{x}_a, \mathbf{x}_b \in \mathcal{X}$, where $\tilde{\mathbf{R}} := \mathbf{R} + n\mathbf{I}_n/\lambda_z$.

Recall $\lambda = \sigma_0^2/(n\sigma^2)$. We have the following predictive distribution of the discretized S-GaSP calibration model.

THEOREM 5.1. *Assume $\delta_{z_d}(\cdot)$ in (5.1) with $p_{Z_d}(\cdot)$ and $g_{Z_d}(\cdot)$ defined in (3.2) and (3.3), respectively. Conditioning on all the parameters, the predictive distribution of the field data at any $\mathbf{x} \in \mathcal{X}$ by the discretized S-GaSP calibration model in (5.1) is a multivariate normal distribution*

$$y^F(\mathbf{x}) \mid \mathbf{y}^F, \boldsymbol{\theta}, \sigma_0^2, \lambda, \lambda_z \sim MN(\hat{\mu}_{z_d}(\mathbf{x}), \sigma_0^2((n\lambda)^{-1} K_{z_d}^*(\mathbf{x}, \mathbf{x}) + 1)),$$

where

$$\begin{aligned}\hat{\mu}_{z_d}(\mathbf{x}) &= f^M(\mathbf{x}, \boldsymbol{\theta}) + \frac{\mathbf{r}^T(\mathbf{x})}{1 + \lambda\lambda_z} \left(\mathbf{R} + \frac{n\lambda}{1 + \lambda\lambda_z} \mathbf{I}_n \right)^{-1} (\mathbf{y}^F - \mathbf{f}_{\boldsymbol{\theta}}^M), \\ K_{z_d}^*(\mathbf{x}, \mathbf{x}) &= K(\mathbf{x}, \mathbf{x}) - \mathbf{r}^T(\mathbf{x}) \left[\mathbf{I}_n + \left(\mathbf{R} + \frac{n\lambda}{1 + \lambda\lambda_z} \mathbf{I}_n \right)^{-1} \frac{n}{(1 + \lambda\lambda_z)\lambda_z} \right] \tilde{\mathbf{R}}^{-1} \mathbf{r}(\mathbf{x}),\end{aligned}$$

where $\mathbf{r}(\mathbf{x}) = (K(\mathbf{x}, \mathbf{x}_1), \dots, K(\mathbf{x}, \mathbf{x}_n))^T$ and $\tilde{\mathbf{R}} = \mathbf{R} + \frac{n}{\lambda_z} \mathbf{I}_n$ with the (i, j) entry of \mathbf{R} being $K(\mathbf{x}_i, \mathbf{x}_j)$.

Theorem 5.1 indicates that the predictive mean of the discretized S-GaSP calibration model shrinks the predictive mean towards the mean function. When $\lambda_z = 0$, the shrinkage is zero and the discretized S-GaSP becomes the GaSP.

Interestingly, when the observations contain no noise, the predictive mean and variance of the field data from the GaSP calibration model and the discretized S-GaSP calibration model are *exactly* the same, stated in the following Lemma 5.1.

LEMMA 5.1. *Assume the same conditions in Theorem 5.1 hold. If $\sigma_0^2 = 0$, the predictive distribution of the field data at any $\mathbf{x} \in \mathcal{X}$ by the discretized S-GaSP model in (5.1) is a multivariate normal distribution with the predictive mean and variance of the field data at any $\mathbf{x} \in \mathcal{X}$ as follows*

$$\begin{aligned}\mathbb{E}[y^F(\mathbf{x}) \mid \mathbf{y}^F, \boldsymbol{\theta}, \lambda, \lambda_z] &= f^M(\mathbf{x}, \boldsymbol{\theta}) + \mathbf{r}^T(\mathbf{x}) \mathbf{R}^{-1} (\mathbf{y}^F - \mathbf{f}_{\boldsymbol{\theta}}^M), \\ \mathbb{V}[y^F(\mathbf{x}) \mid \mathbf{y}^F, \boldsymbol{\theta}, \lambda, \lambda_z] &= \sigma^2 (K(\mathbf{x}, \mathbf{x}) - \mathbf{r}^T(\mathbf{x}) \mathbf{R}^{-1} \mathbf{r}(\mathbf{x})),\end{aligned}$$

where $\mathbf{r}(\mathbf{x}) = (K(\mathbf{x}, \mathbf{x}_1), \dots, K(\mathbf{x}, \mathbf{x}_n))^T$ and \mathbf{R} is an $n \times n$ matrix with the (i, j) entry being $K(\mathbf{x}_i, \mathbf{x}_j)$.

5.1. *Parameter estimation.* In the previous discussion, we treat the kernel function as known and let the regularization parameter λ change along with the number of observations to guarantee the convergence of the predictor. In practice, these parameters are often estimated for better predictive performance. We discuss this issue in this section.

For any $\mathbf{x}_a = (x_{a1}, \dots, x_{ap})^T$ and $\mathbf{x}_b = (x_{b1}, \dots, x_{bp})^T$, the correlation is typically assumed to have a product form in mathematical model calibration

$$(5.3) \quad K(\mathbf{x}_a, \mathbf{x}_b) = \prod_{i=1}^p K_i(d_i),$$

where $d_i = |x_{ai} - x_{bi}|$ for $i = 1, \dots, p$ and $K_i(\cdot)$ is a one dimensional kernel function. One widely used kernel function is the Matérn kernel as follows [13]

$$(5.4) \quad K_i(d_i) = \frac{1}{2^{\nu_i-1}\Gamma(\nu_i)} \left(\frac{d_i}{\gamma_i}\right)^{\nu_i} \mathcal{K}_{\nu_i}\left(\frac{d_i}{\gamma_i}\right),$$

where $\Gamma(\cdot)$ is the gamma function and $\mathcal{K}_{\nu_i}(\cdot)$ is the modified Bessel function of the second kind with a roughness parameter ν_i and a range parameter γ_i for $i = 1, \dots, p$. The sample path of a GaSP with the Matérn kernel is $\lfloor \nu_i - 1 \rfloor$ times differentiable. When $\nu_i = (2k_i + 1)/2$ with $k_i \in \mathbb{N}$, the Matérn kernel has an explicit expression. For example, the Matérn kernel with $\nu_i = 5/2$ has the following form

$$(5.5) \quad K_i(d_i) = \left(1 + \frac{\sqrt{5}d_i}{\gamma_i} + \frac{5d_i^2}{3\gamma_i^2}\right) \exp\left(-\frac{\sqrt{5}d_i}{\gamma_i}\right),$$

for $i = 1, \dots, p$. For the demonstration purpose, we implement all the numerical studies using the product correlation in (5.3) with $K_i(\cdot)$ in (5.5). More benefits of using the Matérn correlation to model the mathematical model outputs are discussed in [12].

Denote $\boldsymbol{\gamma} = (\gamma_1, \dots, \gamma_p)^T$ the unknown range parameters in the covariance. The parameters in the discretized S-GaSP calibration model are the calibration parameters $\boldsymbol{\theta}$, the variance parameter of the noise σ_0^2 , regularization parameter λ , scaling parameter λ_z and range parameters $\boldsymbol{\gamma}$. Simple algebra shows $\hat{\sigma}_{0,MLE}^2 = \lambda S_{z_d}^2$, where $S_{z_d}^2 = (\mathbf{y}^F - \mathbf{f}_{\boldsymbol{\theta}}^M)^T \tilde{\mathbf{R}}_{z_d}^{-1} (\mathbf{y}^F - \mathbf{f}_{\boldsymbol{\theta}}^M)$ with $\tilde{\mathbf{R}}_{z_d} = (\mathbf{R}^{-1} + \lambda_z \mathbf{I}_n/n)^{-1} + \lambda n \mathbf{I}_n$. Marginalizing out $\delta_z(\cdot)$ and plugging $\hat{\sigma}_{0,MLE}^2$ into the likelihood of the discretized S-GaSP calibration model in (5.1), one has the profile likelihood

$$(5.6) \quad \ell_{z_d}(\boldsymbol{\theta}, \boldsymbol{\gamma}, \lambda, \lambda_z) \propto -\frac{1}{2} \log |\tilde{\mathbf{R}}_{z_d}| - \frac{n}{2} \log(S_{z_d}^2).$$

One may numerically maximize the profile likelihood in (5.6) to estimate the parameters. Note λ_z reflects one's tolerance of how good a mathematical model should predict the reality without the discrepancy function and thus this parameter may be chosen based on the expert knowledge. Because of the conditions discussed in Theorem 4.2, λ_z may also be fixed to be proportional to $\lambda^{-1/2}$ or be related to the number of sample size. The Bayesian methods for estimating the parameters are also discussed in [11] and implemented in "RobustCalibration" package on CRAN [8].

Some model parameters in a GaSP model, such as the range and variance parameters, are also unidentifiable in certain scenario when the sampling

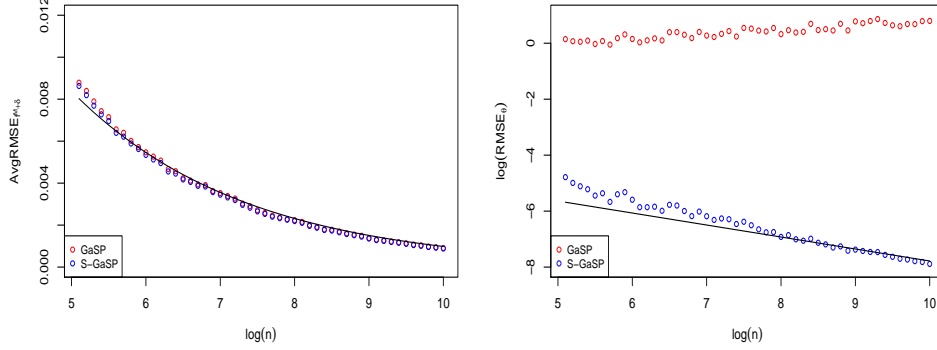


FIG 2. Calibration and prediction for Example 4.1 when the parameters in the GaSP and S-GaSP calibration models are estimated by the MLE. In the left panel, the $\text{AvgRMSE}_{f^{M+\delta}}$ of the GaSP calibration and that of the discretized S-GaSP calibration are graphed as the red and blue circles, respectively; the black curve is $\log(n^{-m/(2m+1)}/14)$, representing the theoretical upper bound by Corollary 4.1 (up to a constant). In the right panel, the natural logarithm of the RMSE_{θ} of the GaSP calibration and that of the discretized S-GaSP calibration are graphed as the red circles and blue circles, respectively; the black line is $\log(n^{-m/(2m+1)}/33)$, representing the theoretical upper bound in Theorem 4.2 (up to a constant). $\lambda_z = \lambda^{-1/2}$ is taken for the S-GaSP calibration.

model is assumed to be a GaSP [37, 38]. The consistent estimation of the model parameters, such as the range parameters, regularization parameter and scaling parameter, is an open problem and a future direction.

The average root of the mean squared error ($\text{AvgRMSE}_{f^{M+\delta}}$) of the prediction in the GaSP and the discretized S-GaSP for Example 4.1 is shown in the left panel in Figure 2, where $\lambda_z = \lambda^{-1/2}$ and $(\theta, \gamma, \lambda)$ are estimated by maximizing the profile likelihood in (5.6). The black curve is the theoretical upper bound up to a constant by Corollary 4.1 with λ and λ_z being fixed to be a function of the sample size. When the parameters are estimated by the MLE, the prediction by the GaSP and the discretized S-GaSP match the theoretical upper bound reasonably well, indicating that the optimal convergence rate is obtained for this example. Compared to the $\text{AvgRMSE}_{f^{M+\delta}}$ with a fixed λ and λ_z in the left panel in Figure 1, both the GaSP and the S-GaSP calibration yields a smaller predictive error when the kernel and regularization parameters are estimated by the MLE. When the sample size is small to moderate, the predictive error in the discretized S-GaSP is slightly smaller than that in the GaSP, as shown in the left panel in Figure 2.

The RMSE_{θ} of the GaSP calibration and that of the S-GaSP calibration

for Example 4.1 are graphed as the red and blue circles in the right panel in Figure 2, respectively. The RMSE_θ of the S-GaSP decreases as the sample size increases, whereas the GaSP calibration does not decrease. Unlike fixing λ as a function of the sample size, the estimated calibration parameters are not guaranteed to converge to the L_2 minimizer when the kernel and regularization parameters in the S-GaSP are estimated by the MLE. For a number of examples shown later, however, we found the estimated calibration parameters from the S-GaSP calibration model are typically very close to the L_2 minimizer.

So far we assume the mathematical model is easy to evaluate. Some mathematical models, however, are computationally expensive. In those cases, one often uses a statistical emulator, often specified as a GaSP, to approximate the mathematical model based on a set of mathematical model runs. The parameter estimation by the MLE of the model parameters in a GaSP emulator is often unstable. The robust marginal posterior mode estimation for the parameters of the GaSP emulator is discussed in [9, 12] and implemented in an “RobustGaSP” package on CRAN [10]. The “RobustGaSP” package is also built in the “RobustCalibration” package [8] for emulating the slow mathematical model in a calibration problem. Due to the limitation of the space, we do not go into the details of the emulation problem.

6. Numerical study.

6.1. *Evaluation criteria.* In this section, we numerically compare the performance of several methods for calibration and prediction. We focus on two loss functions as follows.

- i. The L_2 loss between the reality and the estimator of the reality $L_2(\hat{y}^R(\cdot)) = \|y^R(\cdot) - \hat{y}^R(\cdot)\|_{L_2}^2$.
- ii. The L_2 loss between the reality and calibrated mathematical model $L_2(\hat{\theta}) = \|y^R(\cdot) - f^M(\cdot, \hat{\theta})\|_{L_2}^2$, where $\hat{\theta}$ is the estimator of the calibration parameter.

The first L_2 loss is our primary criterion, because the out of sample prediction for the reality examines how well a calibrated mathematical model and discrepancy function to reproduce the reality. The second criterion follows the arguments in [26, 27, 31], which aims to estimate the calibration parameters such that the L_2 loss between the mathematical model and discrepancy function is minimized. Indeed, the parameters in a mathematical model often have scientific interpretation, whereas the non-linear term in the discrepancy function might be hard to interpret. Thus the discrepancy function is not used for prediction in the second criterion.

In the following simulated examples, we simulate $N = 200$ experiments, where in each experiment, $n^* = 10^4$ outputs from the reality are held out for testing with the inputs uniformly sampled from the input domain. We test on two configurations, where the number of observations is assumed to be $n = 10(p + 1)$ and $n = 20(p + 1)$, both with the inputs generated from the maximin latin hypercube design [24]. We examine the first criterion by $\text{AvgRMSE}_{f_{M+\delta}}$ in Equation (4.6), and the second criterion is examined by

$$(6.1) \quad \text{AvgRMSE}_{f_M} = \frac{1}{N} \sum_{i=1}^N \sqrt{\frac{1}{n^*} \sum_{j=1}^{n^*} (f^M(\mathbf{x}_j^*, \hat{\boldsymbol{\theta}}) - y^R(\mathbf{x}_j^*))^2},$$

where $f^M(\mathbf{x}_j^*, \hat{\boldsymbol{\theta}})$ is the prediction of the mathematical model with the estimated calibration parameters.

We mainly compare the GaSP calibration and the S-GaSP calibration models using $\text{AvgRMSE}_{f_{M+\delta}}$ and AvgRMSE_{f_M} , where the model parameters $(\boldsymbol{\theta}, \boldsymbol{\gamma}, \lambda)$ are estimated by maximizing the profile likelihood. We test two S-GaSP calibration models. In the first model, we let the scaled parameter be $\lambda_z = \lambda^{-1/2}$ and in the second model, we let the scaled parameter be $\lambda_z = 100n^{1/2}$. Two frequentists approaches aiming to find the L_2 minimizer are also compared in the second example. The numerical optimization for the MLE is implemented using the low-storage quasi-Newton optimization method [19] based on 10 different initializations.

6.2. Simulated examples.

EXAMPLE 6.1. Assume $y^F(\mathbf{x}) = y^R(\mathbf{x}) + \epsilon$ with $\epsilon \stackrel{i.i.d.}{\sim} N(0, 0.05^2)$. We test the following four cases (implemented in [25]).

- i. Damped Cosine function from [24], $y^R(x) = \exp(-1.4x) \cos(3.5\pi x)$ and $f^M(x, \boldsymbol{\theta}) = \theta_1 + \theta_2 x$ with $x \in [0, 1]$.
- ii. Cheng & Sandu function from [5], $y^R(\mathbf{x}) = \cos(x_1 + x_2) \exp(x_1 + x_2)$ and $f^M(\mathbf{x}, \boldsymbol{\theta}) = \theta_1 + \theta_2 x_1$ with $x_i \in [0, 1]$ for $i = 1, 2$.
- iii. Morokoff & Catflisch function from [18], $y^R(\mathbf{x}) = (1 + 1/3)^3 \prod_{i=1}^3 x_i^{1/3}$ and $f^M(\mathbf{x}, \boldsymbol{\theta}) = \theta$ with $x_i \in [0, 1]$ for $i = 1, 2, 3$.
- iv. Xiong's low fidelity function from [33], $y^R(\mathbf{x}) = 2/3 \exp(x_1 + x_2) + x_3 - x_4 \sin(x_3)$ and $f^M(\mathbf{x}, \boldsymbol{\theta}) = \theta_1 + \theta_2 x_2 + \theta_3 x_3$ with $x_i \in [0, 1]$ for $i = 1, 2, 3, 4$.

The mathematical models in Example 6.1 are assumed to be either a mean parameter or a linear term. One reason is that the linear term is of particular

$n = 10(p + 1)$	AvgRMSE $_{f_M + \delta}$			AvgRMSE $_{f_M}$		
	GaSP	S-GaSP 1	S-GaSP 2	GaSP	S-GaSP 1	S-GaSP 2
Case (i)	.0383	.0377	.0377	.519	.405	.405
Case (ii)	.0374	.0354	.0353	.664	.281	.281
Case (iii)	.0786	.0757	.0758	1.55	.463	.463
Case (iv)	.0458	.0430	.0433	2.04	.738	.741
$n = 20(p + 1)$	AvgRMSE $_{f_M + \delta}$			AvgRMSE $_{f_M}$		
	GaSP	S-GaSP 1	S-GaSP 2	GaSP	S-GaSP 1	S-GaSP 2
Case (i)	.0263	.0258	.0257	.519	.404	.404
Case (ii)	.0254	.0245	.0243	.828	.279	.279
Case (iii)	.0586	.0563	.0564	2.01	.463	.463
Case (iv)	.0298	.0285	0.288	2.95	.735	.740

TABLE 1

Predictive errors of different methods for four cases in Example 6.1. The GaSP and the S-GaSP denote the GaSP calibration model and the discretized S-GaSP calibration model in (1.2) and (5.1), respectively. The number of observations is assumed to be $n = 10(p + 1)$ and $n = 20(p + 1)$ the first four rows and last four rows, respectively. The AvgRMSE $_{f_M}$ of the L_2 minimizers for case i to case iv is 0.404, 0.277, 0.462 and 0.729, respectively. $\lambda_z = \lambda^{-1/2}$ and $\lambda_z = 100n^{1/2}$ are assumed in the first S-GaSP approach and second S-GaSP approach, respectively.

interest in some studies, such as modeling spatially correlated data and time-dependent outcomes. Some numerical examples for comparing the GaSP and the S-GaSP calibration using mathematical models with nonlinear outcomes are analyzed in [11] and we will provide one example later.

The AvgRMSE $_{f_M + \delta}$ and AvgRMSE $_{f_M}$ in the GaSP and the S-GaSP calibration are shown in the Table 1. First of all, both S-GaSP approaches perform slightly better than the GaSP approach in terms of AvgRMSE $_{f_M + \delta}$ and much better than the GaSP model in terms of AvgRMSE $_{f_M}$ for all examples. The AvgRMSE $_{f_M}$ in the S-GaSP calibration is very close to the one of the L_2 minimizer and decreases when the sample size increases, whereas the AvgRMSE $_{f_M}$ in the GaSP calibration is much larger and does not decrease as the sample size increases.

Figure 3 shows the boxplots of the calibrated parameters of the GaSP and the S-GaSP for case iv in Example 6.1. The calibrated parameters in the two S-GaSP approaches are close to the L_2 minimizer, whereas the first two parameters in the GaSP model are estimated far from the L_2 minimizer. The RMSE $_{\theta}$ of the S-GaSP calibration is much smaller than that of the GaSP calibration. When the sample size increases, the RMSE $_{\theta}$ of the S-GaSP decreases, whereas the RMSE $_{\theta}$ of the GaSP calibration slightly increases.

In the next example, we compare the GaSP and the S-GaSP calibration when the mathematical model is non-linear. We also include two recent two-step calibration methods that seek to find the L_2 minimizer for comparison.

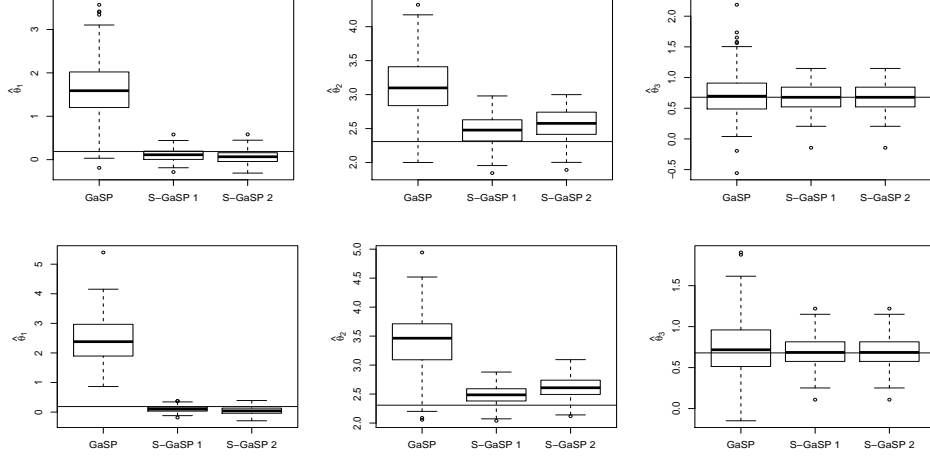


FIG 3. Calibrated parameters using the GaSP and the S-GaSP calibration methods for case *iv* in Example 6.1 with $n = 50$ and $n = 100$ are graphed in the first row and second row, respectively. The black horizontal lines are the L_2 minimizers.

The first two-step approach is the L_2 calibration [26], where the reality is first estimated via a nonparametric regression (chosen as a GaSP model here), and the calibration parameters are estimated by plugging-in the estimator of the reality and minimizing the L_2 loss. The second two-step approach is the least squares (LS) calibration [31], where the calibration parameters are first estimated by minimizing the squared difference between the experimental data and mathematical model, and then the residuals are modeled by a GaSP model for predicting the reality.

EXAMPLE 6.2. Let $y^F(\mathbf{x}) = y^R(\mathbf{x}) + \epsilon$, where $\mathbf{x} = (x_1, x_2) \in [0, 1]^2$, $y^R(\mathbf{x}) = \sin(0.2\pi x_1)x_2 + \sin(2\pi x_1)x_2 + 1$ and $\epsilon \stackrel{i.i.d.}{\sim} N(0, 0.1^2)$. The mathematical model is $f^M(\mathbf{x}, \boldsymbol{\theta}) = \sin(\theta_1 x_1)x_2 + \theta_2$.

We consider two configurations for Example 6.2, where the sample sizes are taken to be $n = 30$ and $n = 60$, respectively. The predictive errors of different methods for Example 6.2 are tabulated in Table 2. For both configurations, the $\text{AvgRMSE}_{f^M+\delta}$ in the S-GaSP calibration with $\lambda_z = \lambda^{-1/2}$ is the smallest, and the GaSP also yields a small $\text{AvgRMSE}_{f^M+\delta}$, almost as good as two S-GaSP approaches.

The $\text{AvgRMSE}_{f^M+\delta}$ of the two-step estimation methods are much larger

n=30	GaSP	S-GaSP 1	S-GaSP 2	L_2	LS
AvgRMSE $_{f^M+\delta}$.0568	.0552	.0570	.0834	.0617
AvgRMSE $_{f^M}$.137	.131	.132	.129	.129
n=60	GaSP	S-GaSP 1	S-GaSP 2	L_2	LS
AvgRMSE $_{f^M+\delta}$.0376	.0371	.0371	.0562	.0390
AvgRMSE $_{f^M}$.138	.130	.131	.126	.126

TABLE 2

Predictive errors by different methods for Example 6.2. The GaSP and the S-GaSP denotes the GaSP calibration model and the discretized S-GaSP in (1.2) and (5.1), respectively. The L_2 and LS denote the two-step calibration methods introduced in [26] and [31], respectively. $\lambda_z = \lambda^{-1/2}$ and $\lambda_z = 100n^{1/2}$ are taken in the first S-GaSP approach and the second S-GaSP approach, respectively.

than those of the GaSP and the S-GaSP calibration for Example 6.2. For the L_2 calibration, since it does not use the mathematical model to predict the reality, the high frequency term $\sin(2\pi x_1)x_2$ makes the predictive error of the nonparametric regression large. This term, however, can be explained by the mathematical model when θ_1 is estimated near 2π , and consequently, the residuals are much easier to be captured by the discrepancy function. The LS calibration does not perform as good as the first two methods either, because the L_2 minimizer of θ_1 is around 6.48, which is larger than 2π . Because the model complexity is not accounted by the calibrated mathematical model, the prediction based on the residuals is not as good as the approaches that simultaneously estimate the parameters and make the prediction, i.e., the GaSP and the S-GaSP calibration model.

The estimated calibration parameters of Example 6.2 using different models are graphed in Figure 4. In the left panel, the estimation of θ_1 using the LS and the L_2 method is close to the L_2 minimizer (graphed as the solid line), whereas the estimation of θ_1 using the GaSP and the S-GaSP is, in fact, closer to 2π , graphed as the dashed line. This is because the model complexity is naturally built into the calibration: an estimated θ_1 that is close to 2π makes the prediction better, since the high frequency term is explained by the mathematical model. The estimation of θ_2 is graphed in the right panel in Figure 6.2. The S-GaSP, the L_2 , and the LS calibration estimate the calibration parameters similarly, whereas the estimates using the GaSP model are quite different. The GaSP calibration produces the largest AvgRMSE $_{f^M}$, whereas the S-GaSP, the LS, and the L_2 calibration yield much smaller AvgRMSE $_{f^M}$, as illustrated in Table 2.

Example 6.2 indicates that the L_2 minimizer might not always be the optimal choice to separate the mathematical model and discrepancy, though one does not expect the calibration to deviate too much from the L_2 mini-

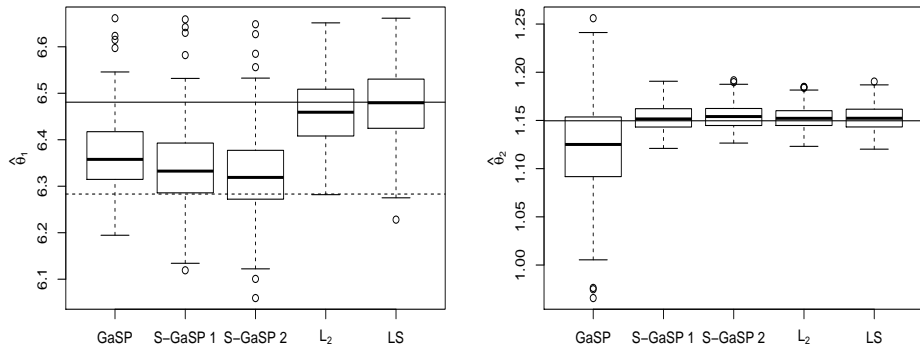


FIG 4. *Boxplots of the estimated calibration parameters from the GaSP, the S-GaSP, L_2 and LS calibration approaches for Example 6.2. $N = 200$ experiments are implemented and $n = 60$ observations are used for calibration in each experiment. The solid lines are the L_2 minimizer, which is around 6.48 and 1.15 for θ_1 and θ_2 , respectively. The dashed line in the left panel is 2π . $\lambda_z = \lambda^{-1/2}$ and $\lambda_z = 100n^{1/2}$ are assumed in the first S-GaSP approach and the second S-GaSP approach, respectively.*

mizer as well. The S-GaSP calibration model seems to do well in both sides. It predicts the reality as accurately as the GaSP calibration model with the assistance of the calibrated mathematical model. The calibrated mathematical model using the S-GaSP is also closer to the reality than the one using the GaSP calibration.

7. Concluding remarks. We have introduced the scaled Gaussian stochastic process (S-GaSP) for the calibration and prediction. We showed that under certain regularity conditions, the predictive mean of the S-GaSP calibration model converges to the reality as fast as the GaSP calibration with some suitable choice of the regularization parameter and scaling parameter. The MLE of the calibration parameters in the S-GaSP converges to the L_2 minimizer with the same choice of the regularization parameter and scaling parameter, whereas the estimated calibration parameters in the GaSP model typically do not converge to the L_2 minimizer. The results rely on the explicit connection between the GaSP and the S-GaSP via the orthogonal series representation and the KRR estimator, both of which are studied in this work. The numerical studies demonstrate that the S-GaSP is better than the GaSP in both out-of-sample prediction and the estimation

of the parameters using the L_2 loss.

The computation of the S-GaSP relies on the discretization of the integral constraint. We did not study the convergence of the discretized S-GaSP, but the numerical studies indicate the convergence rate from the discretized S-GaSP is the same as the S-GaSP. Furthermore, all parameters, including the regularization parameters and the range parameters in the kernel function are often estimated by the MLE or a Bayesian method in practice, the convergence of which in such setting is also unknown. Lastly, one might extend the S-GaSP framework to Markov field for spatially correlated data, to overcome the computational bottleneck when the sample size is large.

Appendix A Proof for Section 2.

PROOF OF LEMMA 2.1. By the representer lemma [21, 30], for any $\boldsymbol{\theta} \in \boldsymbol{\Theta}$ and $\mathbf{x} \in \mathcal{X}$, one has

$$(A.1) \quad \hat{\delta}_{\lambda, n, \boldsymbol{\theta}}(\mathbf{x}) = \sum_{i=1}^n w_i(\boldsymbol{\theta}) K(\mathbf{x}_i, \mathbf{x}).$$

Denote $\mathbf{w}_{\boldsymbol{\theta}} = (w_1(\boldsymbol{\theta}), \dots, w_n(\boldsymbol{\theta}))^T$. Since $\langle K(\mathbf{x}_i, \cdot), K(\mathbf{x}_j, \cdot) \rangle_{\mathcal{H}} = K(\mathbf{x}_i, \mathbf{x}_j)$, (2.7) becomes to find $\boldsymbol{\theta}$ and $\mathbf{w}_{\boldsymbol{\theta}}$ that minimize

$$(A.2) \quad \frac{1}{n}(\mathbf{y}^F - \mathbf{f}_{\boldsymbol{\theta}}^M - \mathbf{R}\mathbf{w}_{\boldsymbol{\theta}})^T(\mathbf{y}^F - \mathbf{f}_{\boldsymbol{\theta}}^M - \mathbf{R}\mathbf{w}_{\boldsymbol{\theta}}) + \lambda \mathbf{w}_{\boldsymbol{\theta}}^T \mathbf{R} \mathbf{w}_{\boldsymbol{\theta}}.$$

For any $\boldsymbol{\theta}$, solving the minimization for (A.2) with regard to $\mathbf{w}_{\boldsymbol{\theta}}$ gives

$$(A.3) \quad \hat{\mathbf{w}}_{\boldsymbol{\theta}} = (\mathbf{R} + n\lambda \mathbf{I}_n)^{-1}(\mathbf{y}^F - \mathbf{f}_{\boldsymbol{\theta}}^M).$$

Then plugging $\hat{\mathbf{w}}_{\boldsymbol{\theta}}$ into (A.2), based on the Woodbury matrix identity, one has

$$\begin{aligned} & \frac{1}{n}(\mathbf{y}^F - \mathbf{f}_{\boldsymbol{\theta}}^M - \mathbf{R}\hat{\mathbf{w}}_{\boldsymbol{\theta}})^T(\mathbf{y}^F - \mathbf{f}_{\boldsymbol{\theta}}^M - \mathbf{R}\hat{\mathbf{w}}_{\boldsymbol{\theta}}) + \lambda \hat{\mathbf{w}}_{\boldsymbol{\theta}}^T \mathbf{R} \hat{\mathbf{w}}_{\boldsymbol{\theta}} \\ &= \frac{1}{n}(\mathbf{y}^F - \mathbf{f}_{\boldsymbol{\theta}}^M)^T [(\mathbf{I}_n - \mathbf{R}(\mathbf{R} + n\lambda \mathbf{I}_n)^{-1})^T (\mathbf{I}_n - \mathbf{R}(\mathbf{R} + n\lambda \mathbf{I}_n)^{-1})] \\ & \quad + \lambda (\mathbf{y}^F - \mathbf{f}_{\boldsymbol{\theta}}^M)^T (\mathbf{R} + n\lambda \mathbf{I}_n)^{-1} \mathbf{R} (\mathbf{R} + n\lambda \mathbf{I}_n)^{-1} (\mathbf{y}^F - \mathbf{f}_{\boldsymbol{\theta}}^M) \\ (A.4) \quad &= \lambda (\mathbf{y}^F - \mathbf{f}_{\boldsymbol{\theta}}^M)^T (\mathbf{R} + n\lambda \mathbf{I}_n)^{-1} (\mathbf{y}^F - \mathbf{f}_{\boldsymbol{\theta}}^M), \end{aligned}$$

which shows that the minimizer of $\boldsymbol{\theta}$ on right-hand side of (A.4) is the same as the MLE of $\boldsymbol{\theta}$ in (2.5). Finally, plugging the estimator $\hat{\boldsymbol{\theta}}_{\lambda, n}$ into (A.2), the result follows from the KRR estimator of $\delta(\cdot)$ in (A.1) with the weights in (A.3). \square

Appendix B Proof for Section 3.

PROOF OF LEMMA 3.1. By Karhunen-Loève expansion, we have

$$\delta(\mathbf{x}) = \sigma \sum_{i=1}^{\infty} \sqrt{\rho_i} Z_i \phi_i(\mathbf{x})$$

with $Z_i \stackrel{i.i.d}{\sim} N(0, 1)$. Denote $W_k = \sum_{i=k+1}^{\infty} \rho_i Z_i^2$ for any $k \in \mathbb{N}^+$. From the definition of $Z = \int_{\mathbf{x} \in \mathcal{X}} \delta^2(\mathbf{x}) d\mathbf{x}$ and $\int_{\mathbf{x} \in \mathcal{X}} \phi_i^2(\mathbf{x}) d\mathbf{x} = 1$ for any $i \in \mathbb{N}^+$, it is straightforward to see that

$$(B.1) \quad Z = \sigma^2(\rho_1 Z_1^2 + \cdots + \rho_k Z_k^2 + W_k).$$

In the following expressions, we are conditioning on all parameters and they are dropped for simplicity. From the construction of

$$\delta_z(\mathbf{x}) = \left\{ \delta(\mathbf{x}) \mid \int_{\mathbf{x} \in \mathcal{X}} \delta^2(\mathbf{x}) d\mathbf{x} = Z \right\}$$

and $Z \sim p_Z(\cdot)$, the joint density of (Z_1, \dots, Z_k, W_k) in the S-GaSP can be expressed as

$$\begin{aligned} & p_{\delta_z}(Z_1 = z_1, \dots, Z_k = z_k, W_k = w_k) \\ &= \int_0^{\infty} p_{\delta}(Z_1 = z_1, \dots, Z_k = z_k, W_k = w_k \mid Z = z) p_Z(Z = z) dz \\ &\propto \int_0^{\infty} \frac{p_{\delta}(Z = z, Z_1 = z_1, \dots, Z_k = z_k, W_k = w_k)}{p_{\delta}(Z = z)} g_Z(Z = z) p_{\delta}(Z = z) dz \\ &\propto p_{\delta}(Z_1 = z_1, \dots, Z_k = z_k) p_{\delta}(W_k = w_k) \times \\ &\quad \int_0^{\infty} p_{\delta}(Z = z \mid Z_1 = z_1, \dots, Z_k = z_k, W_k = w_k) \exp\left(-\frac{\lambda_z z}{2\sigma^2}\right) dz \\ &\propto p_{\delta}(Z_1 = z_1, \dots, Z_k = z_k) p_{\delta}(W_k = w_k) \times \\ &\quad \int_0^{\infty} \mathbb{1}\left\{z = \sigma^2(\rho_1 z_1^2 + \cdots + \rho_k z_k^2 + w_k)\right\} \exp\left(-\frac{\lambda_z z}{2\sigma^2}\right) dz \\ &\propto \exp\left(-\frac{1}{2} \sum_{i=1}^k z_i^2\right) p_{\delta}(W_k = w_k) \exp\left[-\frac{\lambda_z}{2} \left(\sum_{i=1}^k \rho_i z_i^2 + w_k\right)\right] \\ &= \left\{ \prod_{i=1}^k \exp\left[-\frac{1}{2}(1 + \lambda_z \rho_i) z_i^2\right] \right\} p_{\delta}(W_k = w_k) \exp(-\lambda_z w_k/2). \end{aligned}$$

After integrating out W_k , it is clear that Z_i 's are independently distributed as $N(0, 1/(1 + \lambda_z \rho_i))$ under the measure induced by the S-GaSP. Since k is arbitrary, we have

$$\delta_z(\mathbf{x}) = \sigma \sum_{i=1}^{\infty} \sqrt{\frac{\rho_i}{1 + \lambda_z \rho_i}} Z_i \phi_i(\mathbf{x})$$

with $Z_i \stackrel{i.i.d.}{\sim} N(0, 1)$, from which the proof is complete. \square

PROOF OF LEMMA 3.2. First note that for any $\mathbf{x}_a, \mathbf{x}_b \in \mathcal{X}$, we have $K(\mathbf{x}_a, \mathbf{x}_b) = \sum_{i=1}^{\infty} \rho_i \phi_i(\mathbf{x}_a) \phi_i(\mathbf{x}_b)$ and $K_z(\mathbf{x}_a, \mathbf{x}_b) = \sum_{i=1}^{\infty} \rho_{z,i} \phi_i(\mathbf{x}_a) \phi_i(\mathbf{x}_b)$ with $\rho_{z,i} = \rho_i / (1 + \lambda_z \rho_i)$. For $h(\cdot) = \sum_{i=1}^{\infty} h_i \phi_i(\cdot) \in \mathcal{H}$ and $g(\cdot) = \sum_{i=1}^{\infty} g_i \phi_i(\cdot) \in \mathcal{H}$, one has

$$\langle h, g \rangle_{\mathcal{H}_z} = \sum_{i=1}^{\infty} \frac{1}{\rho_{z,i}} h_i g_i = \sum_{i=1}^{\infty} \frac{1}{\rho_i} h_i g_i + \lambda_z \sum_{i=1}^{\infty} h_i g_i = \langle h, g \rangle_{\mathcal{H}} + \lambda_z \langle h, g \rangle_{L_2}.$$

\square

PROOF OF LEMMA 3.3. We show below that for any $\boldsymbol{\theta} \in \boldsymbol{\Theta}$ and any $\mathbf{x} \in \mathcal{X}$, one has

$$(B.2) \quad \hat{\delta}_{\lambda, \lambda_z, n}(\mathbf{x}) = \sum_{i=1}^n w_{z,i}(\boldsymbol{\theta}) K_z(\mathbf{x}_i, \mathbf{x}).$$

For any $\delta(\cdot) \in \mathcal{H}$, decomposing it into the linear combination of the basis $\{\lambda_z K_z(\mathbf{x}_i, \cdot)\}_{i=1}^n$ and the orthogonal complement $v(\cdot)$ gives

$$\delta(\cdot) = \sum_{i=1}^n \tilde{w}_{z,i}(\boldsymbol{\theta}) \lambda_z K_z(\mathbf{x}_i, \cdot) + v(\cdot),$$

where $\langle v(\cdot), \lambda_z K_z(\cdot, \mathbf{x}_i) \rangle_{\mathcal{H}_z} = 0$ for $i = 1, \dots, n$.

To evaluate $\delta(\cdot)$ at \mathbf{x}_j for any $j = 1, \dots, n$, we have

$$\begin{aligned} \delta(\mathbf{x}_j) &= \left\langle \sum_{i=1}^n \tilde{w}_{z,i}(\boldsymbol{\theta}) \lambda_z K_z(\mathbf{x}_i, \cdot) + v(\cdot), K_z(\mathbf{x}_j, \cdot) \right\rangle_{\mathcal{H}_z} \\ &= \sum_{i=1}^n \tilde{w}_{z,i}(\boldsymbol{\theta}) \lambda_z K_z(\mathbf{x}_i, \mathbf{x}_j), \end{aligned}$$

which is independent from $v(\cdot)$. Hence the first term on right-hand side of (3.7) is also independent from $v(\cdot)$. For the second term on right-hand side

of (3.7), since $v(\cdot)$ is orthogonal to $\{K_z(\mathbf{x}_i, \cdot)\}_{i=1}^n$, plugging in the decomposition of $\delta(\cdot)$, we have

$$\begin{aligned} \lambda \|\delta\|_{\mathcal{H}_z}^2 &= \lambda \left(\left\| \sum_{i=1}^n \tilde{w}_{z,i}(\boldsymbol{\theta}) \lambda_z K_z(\mathbf{x}_i, \cdot) \right\|_{\mathcal{H}_z}^2 + \|v\|_{\mathcal{H}_z}^2 \right) \\ &\geq \lambda \left\| \sum_{i=1}^n \tilde{w}_{z,i}(\boldsymbol{\theta}) \lambda_z K_z(\mathbf{x}_i, \cdot) \right\|_{\mathcal{H}_z}^2. \end{aligned}$$

Thus choosing $v(\cdot) = 0$ does not change the first term on right-hand side of (3.7), but also minimizes the second term on right-hand side of (3.7). Letting $w_{z,i}(\boldsymbol{\theta}) = \tilde{w}_{z,i}(\boldsymbol{\theta}) \lambda_z$, we have proved (B.2). The rest of the proof can be derived similarly as the proof for Lemma 2.1, so it is omitted here. \square

Appendix C Proof for Section 4.1. We prove Theorem 4.1 in this Section. Two auxillary Lemmas used for the proof of Theorem 4.1 are given after the proof.

Proof for Theorem 4.1. Define a new inner product on \mathcal{H} as

$$(C.1) \quad \langle f, g \rangle_\lambda = (1 + \sqrt{\lambda}) \langle f, g \rangle_{L_2(\mathcal{X})} + \lambda \langle f, g \rangle_{\mathcal{H}}$$

Let $f = \sum_{k=1}^\infty f_k \phi_k$ and $g = \sum_{k=1}^\infty g_k \phi_k$ be elements in \mathcal{H} . Then

$$\langle f, g \rangle_\lambda = (1 + \sqrt{\lambda}) \sum_{k=1}^\infty f_k g_k + \lambda \sum_{k=1}^\infty \frac{f_k g_k}{\rho_k} = \sum_{k=1}^\infty \left(1 + \sqrt{\lambda} + \frac{\lambda}{\rho_k} \right) f_k g_k.$$

By letting μ_k by $\mu_k^{-1} = 1 + \sqrt{\lambda} + \lambda/\rho_k$, we can define a new reproducing kernel

$$(C.2) \quad K_\lambda(\mathbf{x}, \mathbf{x}') = \sum_{k=1}^\infty \mu_k \phi_k(\mathbf{x}) \phi_k(\mathbf{x}')$$

Since $c_\rho^{-1} k^{-2m/p} \leq \rho_k \leq C_\rho^{-1} k^{-2m/p}$ and $|\phi_i(\cdot)| < C_\phi$ for some positive constants c_ρ , C_ρ and C_ϕ , bounding the sums by integrals, we have

$$\begin{aligned} \sup_{\mathbf{x}, \mathbf{x}'} K_\lambda(\mathbf{x}, \mathbf{x}') &\leq C_\phi^2 \sum_{k=1}^\infty \frac{1}{1 + \lambda c_\rho k^{2m/p}} \leq C_\phi^2 \sum_{k=1}^\infty \int_{k-1}^k \frac{1}{1 + \lambda c_\rho x^{2m/p}} dx \\ &= C_\phi^2 c_\rho^{-p/2m} \lambda^{-p/2m} \int_0^\infty \frac{(\lambda c_\rho)^{p/2m}}{1 + \{(\lambda c_\rho)^{p/2m} x\}^{2m/p}} dx \\ &= C_\phi^2 c_\rho^{-p/2m} \lambda^{-p/2m} \int_0^\infty \frac{1}{1 + x^{2m/p}} dx. \end{aligned}$$

Thus

$$(C.3) \quad \sup_{\mathbf{x}, \mathbf{x}'} K_\lambda(\mathbf{x}, \mathbf{x}') \leq C_K^2 \lambda^{-p/(2m)},$$

for some constant C_K depending on K . Define the following linear operators $F_\lambda : \mathcal{H} \rightarrow \mathcal{H}$ and $P_\lambda : \mathcal{H} \rightarrow \mathcal{H}$ via

$$(F_\lambda g)(\mathbf{x}) = \int_{\mathcal{X}} g(\mathbf{x}') K_\lambda(\mathbf{x}, \mathbf{x}') d\mathbf{x}', \quad \text{and} \quad (P_\lambda g)(\mathbf{x}) = g(\mathbf{x}) - (F_\lambda g)(\mathbf{x}),$$

Clearly, we have

$$(C.4) \quad \begin{aligned} \langle f, F_\lambda g \rangle_\lambda &= \sum_{k=1}^{\infty} \langle f, \phi_k \rangle_{L_2(\mathcal{X})} \langle g, \phi_k \rangle_{L_2(\mathcal{X})} = \langle f, g \rangle_{L_2(\mathcal{X})}, \\ \langle f, P_\lambda g \rangle_\lambda &= \langle f, g \rangle_\lambda - \langle f, F_\lambda g \rangle_\lambda = \sqrt{\lambda} \langle f, g \rangle_{L_2(\mathcal{X})} + \lambda \langle f, g \rangle_{\mathcal{H}}. \end{aligned}$$

Denote the loss function

$$\ell_{n\lambda}(f) = \frac{1}{n} \sum_{i=1}^n (y_i - f(\mathbf{x}_i))^2 + \sqrt{\lambda} \|f\|_{L_2(\mathcal{X})}^2 + \lambda \|f\|_{\mathcal{H}}^2,$$

and the estimator $\hat{f}_{n\lambda} := \arg \min_{f \in \mathcal{H}} \ell_{n\lambda}(f)$. Let $D\ell_{n\lambda}(f) : \mathcal{H} \rightarrow \mathcal{H}$ be the Frechét derivative of $\ell_{n\lambda}$ evaluated at f . Clearly, for any $g \in \mathcal{H}$,

$$(C.5) \quad \begin{aligned} D\ell_{n\lambda}(f)g &= \frac{2}{n} \sum_{i=1}^n (f(\mathbf{x}_i) - y_i) \langle K_\lambda(\mathbf{x}_i, \cdot), g(\cdot) \rangle_\lambda + 2 \langle P_\lambda f, g \rangle_\lambda \\ &= \left\langle \frac{2}{n} \sum_{i=1}^n (f(\mathbf{x}_i) - y_i) K_\lambda(\mathbf{x}_i, \cdot) + 2(P_\lambda f)(\cdot), g(\cdot) \right\rangle_\lambda. \end{aligned}$$

It follows that $D\ell_{n\lambda}(\hat{f}_{n\lambda})g = 0$ for all $g \in \mathcal{H}$, and hence, $S_{n\lambda}(\hat{f}_{n\lambda})(\cdot) = 0$, where

$$S_{n\lambda}(f)(\cdot) = \frac{1}{n} \sum_{i=1}^n (y_i - f(\mathbf{x}_i)) K_\lambda(\mathbf{x}_i, \cdot) - (P_\lambda f)(\cdot).$$

Define $S_\lambda(f)(\cdot) = \mathbb{E}_{y, \mathbf{x}}(S_{n\lambda}(f)(\cdot))$. Then

$$\begin{aligned} S_\lambda(f)(\cdot) &= \int_{\mathbf{x} \in \mathcal{X}} (f_0(\mathbf{x}) - f(\mathbf{x})) K_\lambda(\mathbf{x}, \cdot) d\mathbf{x} - (P_\lambda f)(\cdot) \\ &= (F_\lambda(f_0 - f))(\cdot) - (P_\lambda f)(\cdot) = (F_\lambda f_0)(\cdot) - f(\cdot), \end{aligned}$$

and therefore, $S_\lambda(F_\lambda f_0)(\cdot) = 0$. Let $\Delta f = \hat{f}_{n\lambda} - F_\lambda f_0$. By the definitions of $S_{n\lambda}$ and S_λ , we have

$$\begin{aligned}
 & \left\{ S_{n\lambda}(\hat{f}_{n\lambda}) - S_\lambda(\hat{f}_{n\lambda}) \right\}(\cdot) - \left\{ S_{n\lambda}(F_\lambda f_0) - S_\lambda(F_\lambda f_0) \right\}(\cdot) \\
 &= \left\{ S_{n\lambda}(\hat{f}_{n\lambda}) - S_{n\lambda}(F_\lambda f_0) \right\}(\cdot) - \left\{ S_\lambda(\hat{f}_{n\lambda}) - S_\lambda(F_\lambda f_0) \right\}(\cdot) \\
 &= \frac{1}{n} \sum_{i=1}^n \left\{ F_\lambda f_0(\mathbf{x}_i) - \hat{f}_{n\lambda}(\mathbf{x}_i) \right\} K_\lambda(\mathbf{x}_i, \cdot) + P_\lambda \left\{ (F_\lambda f_0)(\cdot) - \hat{f}_{n\lambda}(\cdot) \right\} \\
 &\quad + \hat{f}_{n\lambda}(\cdot) - (F_\lambda f_0)(\cdot) \\
 &= -\frac{1}{n} \sum_{i=1}^n \Delta f(\mathbf{x}_i) K_\lambda(\mathbf{x}_i, \cdot) - (P_\lambda \Delta f)(\cdot) + (\Delta f)(\cdot) \\
 &= -\frac{1}{n} \sum_{i=1}^n \Delta f(\mathbf{x}_i) K_\lambda(\mathbf{x}_i, \cdot) + \mathbb{E}_{\mathbf{x}} \{ \Delta f(\mathbf{x}) K_\lambda(\mathbf{x}, \cdot) \}.
 \end{aligned}$$

On the other hand, $S_{n\lambda}(\hat{f}_{n\lambda})(\cdot) = S_\lambda(F_\lambda f_0)(\cdot) = 0$ and $S_\lambda(\hat{f}_{n\lambda})(\cdot) = (F_\lambda f_0)(\cdot) - \hat{f}_{n\lambda}(\cdot) = -\Delta f(\cdot)$. Therefore,

$$\left\{ S_{n\lambda}(\hat{f}_{n\lambda}) - S_\lambda(\hat{f}_{n\lambda}) \right\}(\cdot) - \left\{ S_{n\lambda}(F_\lambda f_0) - S_\lambda(F_\lambda f_0) \right\}(\cdot) = \Delta f(\cdot) - S_{n\lambda}(F_\lambda f_0)(\cdot).$$

Define the event

$$A_n(t) = \left\{ \left\| \frac{1}{n} \sum_{i=1}^n g(\mathbf{x}_i) K_\lambda(\mathbf{x}_i, \cdot) - \mathbb{E}_{\mathbf{x}} \{ g(\mathbf{x}) K_\lambda(\mathbf{x}, \cdot) \} \right\|_\lambda < t \|g\|_\lambda \text{ for all } g \in \mathcal{H} \right\}.$$

Applying Lemma C.2 on $g(\cdot)/\|g\|_\lambda$,

$$\mathbb{P}_{\mathbf{x}} \{ A_n(t) \} \geq 1 - 2 \exp \left\{ -\lambda^{p(6m-p)/(4m^2)} \left(\frac{nt^2}{\kappa_K} \right) \right\}$$

for some constant $\kappa_K > 0$. The deviation threshold t will be specified later, and from now we consider data points $(\mathbf{x}_i, y_i)_{i=1}^n$ over the event $A_n(t)$.

Over the event $A_n(t)$, we have

$$\begin{aligned}
 & \left\{ S_{n\lambda}(\hat{f}_{n\lambda}) - S_\lambda(\hat{f}_{n\lambda}) \right\}(\cdot) - \left\{ S_{n\lambda}(F_\lambda f_0) - S_\lambda(F_\lambda f_0) \right\}(\cdot) \\
 &= -\frac{1}{n} \sum_{i=1}^n \Delta f(\mathbf{x}_i) K_\lambda(\mathbf{x}_i, \cdot) + \mathbb{E}_{\mathbf{x}} \{ \Delta f(\mathbf{x}) K_\lambda(\mathbf{x}, \cdot) \} \\
 &= \Delta f(\cdot) - S_{n\lambda}(F_\lambda f_0)(\cdot),
 \end{aligned}$$

implying that

$$\begin{aligned}\|\Delta f - S_{n\lambda}(F_\lambda f_0)\|_\lambda &= \left\| \frac{1}{n} \sum_{i=1}^n \Delta f(\mathbf{x}_i) K_\lambda(\mathbf{x}_i, \cdot) - \mathbb{E}_{\mathbf{x}} \{ \Delta f(\mathbf{x}) K_\lambda(\mathbf{x}, \cdot) \} \right\|_\lambda \\ &\leq t \|\Delta f\|_\lambda.\end{aligned}$$

Now we proceed to bound $\|S_{n\lambda}(F_\lambda f_0)\|_\lambda$. Write

$$\begin{aligned}\|S_{n\lambda}(F_\lambda f_0)\|_\lambda &= \left\| \frac{1}{n} \sum_{i=1}^n \{y_i - F_\lambda f_0(\mathbf{x}_i)\} K_\lambda(\mathbf{x}_i, \cdot) - (P_\lambda F_\lambda f_0)(\cdot) \right\|_\lambda \\ &\leq \left\| \frac{1}{n} \sum_{i=1}^n \{f_0(\mathbf{x}_i) - F_\lambda f_0(\mathbf{x}_i)\} K_\lambda(\mathbf{x}_i, \cdot) - \{F_\lambda(f_0 - F_\lambda f_0)\}(\cdot) \right\|_\lambda \\ &\quad + \left\| \frac{1}{n} \sum_{i=1}^n \epsilon_i K_\lambda(\mathbf{x}_i, \cdot) \right\|_\lambda \\ &= \left\| \frac{1}{n} \sum_{i=1}^n \{f_0(\mathbf{x}_i) - F_\lambda f_0(\mathbf{x}_i)\} K_\lambda(\mathbf{x}_i, \cdot) - \mathbb{E}_{\mathbf{x}} [\{f_0(\mathbf{x}) - F_\lambda f_0(\mathbf{x})\} K_\lambda(\mathbf{x}, \cdot)] \right\|_\lambda \\ &\quad + \left\| \frac{1}{n} \sum_{i=1}^n \epsilon_i K_\lambda(\mathbf{x}_i, \cdot) \right\|_\lambda \\ &\leq t \|f_0 - F_\lambda f_0\|_\lambda + \left\| \frac{1}{n} \sum_{i=1}^n \epsilon_i K_\lambda(\mathbf{x}_i, \cdot) \right\|_\lambda,\end{aligned}$$

where the last inequality is due to the construction of the event $A_n(t)$. To bound the second term of the preceding display, we let $\Sigma_\lambda = [K_\lambda(\mathbf{x}_i, \mathbf{x}_j)]_{n \times n}$ and $\boldsymbol{\epsilon} = [\epsilon_1, \dots, \epsilon_n]^\top$. By the Hanson-Wright inequality [23], for all $x > 0$, we have

$$\mathbb{P}_{\mathbf{x}} \left[\boldsymbol{\epsilon}^\top \Sigma_\lambda \boldsymbol{\epsilon} \geq \sigma_0^2 \left\{ \text{tr}(\Sigma_\lambda) + 2\sqrt{\text{tr}(\Sigma_\lambda^2)}x + 2\|\Sigma_\lambda\|_{\text{F}}x^2 \right\} \right] \leq e^{-x^2}.$$

Since by the Cauchy-Schwarz inequality,

$$\begin{aligned}\text{tr}(\Sigma_\lambda) &= \sum_{i=1}^n \|K_\lambda(\mathbf{x}_i, \cdot)\|_\lambda^2 = \sum_{i=1}^n K_\lambda(\mathbf{x}_i, \mathbf{x}_i) \leq C_K^2 n \lambda^{-p/(2m)}, \\ \text{tr}(\Sigma_\lambda^2) &\leq \sum_{i=1}^n \sum_{j=1}^n \|K_\lambda(\mathbf{x}_i, \cdot)\|_{L_2(\mathcal{X})} \|K_\lambda(\mathbf{x}_j, \cdot)\|_{L_2(\mathcal{X})} \leq C_K^4 n^2 \lambda^{-p/m},\end{aligned}$$

$$\|\Sigma_\lambda\|_F = \sqrt{\text{tr}(\Sigma_\lambda^2)} \leq C_K^2 n \lambda^{-p/(2m)},$$

it follows that

$$(C.6) \quad \text{tr}(\Sigma_\lambda) + 2\sqrt{\text{tr}(\Sigma_\lambda^2)}x + 2\|\Sigma_\lambda\|_F x^2 \leq C_K^2 n \lambda^{-p/(2m)}(1 + 2x + 2x^2).$$

Set the event B_n to be

$$B_n = \left\{ \left\| \frac{1}{n} \sum_{i=1}^n e_i K_\lambda(\mathbf{x}_i, \cdot) \right\|_\lambda < \sigma_0 C_K n^{-1/2} \lambda^{-p/(4m)} \alpha^{1/2} \right\},$$

where $\alpha = 2 + 3x^2$. Since $1 + 2x + 2x^2 \leq 2 + 3x^2 = \alpha$, by taking $x = \sqrt{(\alpha - 2)/3}$, we have $\mathbb{P}(B_n) \geq 1 - \exp(-(\alpha - 2)/3)$ for any $\alpha > 2$. Putting all pieces obtained above together, we have

$$(C.7) \quad \begin{aligned} \|\Delta f\|_\lambda &\leq \|\Delta f - S_{n\lambda}(F_\lambda f_0)\|_\lambda + \|S_{n\lambda}(F_\lambda f_0)\|_\lambda \\ &\leq t\|\Delta f\|_\lambda + t\|f_0 - F_\lambda f_0\|_\lambda + \sigma_0 C_K n^{-1/2} \lambda^{-p/(4m)} \alpha^{1/2} \\ &= t\|\Delta f\|_\lambda + t\|P_\lambda f_0\|_\lambda + \sigma_0 C_K n^{-1/2} \lambda^{-p/(4m)} \alpha^{1/2}, \end{aligned}$$

over the event $A_n(t) \cap B_n$. Now take $\lambda = n^{-2m/(2m+p)}$. Choose any $C_\beta \in (0, 1)$ and let $t = \sqrt{\kappa_K / (n^{(1-C_\beta)\beta} \log(2))}$. Then, for sufficiently large n ,

$$\mathbb{P}_{\mathbf{x}}\{A_n(t)\} \geq 1 - 2 \exp\left\{-\frac{n^\beta t^2}{\kappa_K}\right\} \geq 1 - \exp\left\{-n^{C_\beta \beta}\right\},$$

where $\beta = (2m - p)^2 / (2m(2m + p))$, and therefore,

$$\|\Delta f\|_\lambda \leq \|P_\lambda f_0\|_\lambda + 2\sigma_0 C_K n^{-m/(2m+p)} \alpha^{1/2},$$

with probability at least

$$\begin{aligned} \mathbb{P}\{A_n(t) \cap B_n\} &= 1 - \mathbb{P}\{A_n^c(t) \cup B_n^c\} \\ &\geq 1 - \mathbb{P}\{A_n^c(t)\} - \mathbb{P}(B_n^c) = 1 - \exp\{-(\alpha - 2)/3\} - \exp\{-n^{C_\beta \beta}\} \end{aligned}$$

for sufficiently large n . Observe that

$$\begin{aligned} \|P_\lambda f_0\|_\lambda^2 &= \left\| \sum_{k=1}^{\infty} (1 - \mu_k) \langle f_0, \phi_k \rangle_{L_2(\mathcal{X})} \phi_k(\cdot) \right\|_\lambda^2 = \sum_{k=1}^{\infty} \frac{(1 - \mu_k)^2}{\mu_k} \langle f_0, \phi_k \rangle_{L_2(\mathcal{X})}^2 \\ &= \sum_{k=1}^{\infty} \frac{(\sqrt{\lambda} + \lambda/\rho_k)^2}{1 + \sqrt{\lambda} + \lambda/\rho_k} \langle f_0, \phi_k \rangle_{L_2(\mathcal{X})}^2 \leq \sum_{k=1}^{\infty} \frac{2\lambda + 2(\lambda/\rho_k)^2}{1 + \lambda/\rho_k} \langle f_0, \phi_k \rangle_{L_2(\mathcal{X})}^2 \end{aligned}$$

$$\begin{aligned}
&\leq 2\lambda \sum_{k=1}^{\infty} \langle f_0, \phi_k \rangle_{L_2(\mathcal{X})}^2 + 2\lambda \sum_{k=1}^{\infty} \frac{1}{\rho_k} \langle f_0, \phi_k \rangle_{L_2(\mathcal{X})}^2 \\
&= 2\lambda \|f_0\|_{L_2(\mathcal{X})}^2 + 2\lambda \|f_0\|_{\mathcal{H}}^2 \\
&\leq 2n^{-2m/(2m+p)} (\|f_0\|_{L_2(\mathcal{X})} + \|f_0\|_{\mathcal{H}})^2.
\end{aligned}$$

Hence, we proceed to compute

$$\begin{aligned}
\|\hat{f}_{n\lambda} - f_0\|_{L_2(\mathcal{X})} &\leq \|\hat{f}_{n\lambda} - f_0\|_{\lambda} \\
&\leq \|\hat{f}_{n\lambda} - F_{\lambda}f_0\|_{\lambda} + \|F_{\lambda}f_0 - f_0\|_{\lambda} \\
&= \|\Delta f\|_{\lambda} + \|P_{\lambda}f_0\|_{\lambda} \\
&\leq \left(2\sqrt{2}(\|f_0\|_{L_2(\mathcal{X})} + \|f_0\|_{\mathcal{H}}) + 2\sigma_0 C_K \alpha^{1/2}\right) n^{-m/(2m+p)}
\end{aligned}$$

with probability at least $1 - \exp\{-(\alpha - 2)/3\} - \exp(-n^{C_{\beta}\beta})$ for sufficiently large n . The bound for $\|\hat{f}_{\lambda, \lambda_z, n} - f_0\|_{\mathcal{H}}$ follows immediately by the definition of $\|\cdot\|_{\lambda}$, completing the proof. \square

The following the Lemma C.1 is Theorem 3.6 in [20], which is needed for the proof of Lemma C.2.

LEMMA C.1. *Let $(X_j)_{j=0}^{\infty}$ be a sequence of random elements in a Hilbert space \mathcal{H} with norm $\|\cdot\|_{\mathcal{H}}$. Suppose that $(X_j)_{j=0}^{\infty}$ forms a martingale in the sense that $\mathbb{E}(X_j | X_0, \dots, X_{j-1}) = X_j$ a.s., and that the difference sequence $(D_j)_{j=1}^{\infty} = (X_j - X_{j-1})_{j=1}^{\infty}$ satisfies $\|D_j\|_{\mathcal{H}}^2 \leq b_j^2$ a.s. and $\sum_{j=1}^{\infty} b_j^2 \leq b_*^2$. Then for any $t \geq 0$,*

$$\mathbb{P}\left(\sup_{j \geq 1} \|X_j\|_{\mathcal{H}} \geq t\right) \leq 2 \exp\left(-\frac{t^2}{2b_*^2}\right).$$

The following maximum inequality for functional empirical processes in the Sobolev space $\mathcal{W}_2^m(\mathcal{X}, 1)$, which generalizes Lemma 5.1 in [34] to multivariate functions, is of fundamental importance to the proof of Theorem 4.1.

LEMMA C.2. *Denote $\mathcal{W}_2^m(\mathcal{X}, 1) = \{f \in \mathcal{W}_2^m(\mathcal{X}) : \|f\|_{\lambda} \leq 1\}$. Suppose $\mathbf{x}_1, \dots, \mathbf{x}_n$ are independently and uniformly drawn from \mathcal{X} . Then there exists some constant κ_K depending on the kernel K , such that for any $t > 0$,*

$$\begin{aligned}
&\mathbb{P}_{\mathbf{x}}\left(\sup_{g \in \mathcal{W}_2^m(\mathcal{X}, 1)} \left\| \frac{1}{n} \sum_{i=1}^n [g(\mathbf{x}_i) K_{\lambda}(\mathbf{x}_i, \cdot) - \mathbb{E}_{\mathbf{x}} \{g(\mathbf{x}) K_{\lambda}(\mathbf{x}, \cdot)\}] \right\|_{\lambda} \geq t\right) \\
&\leq 2 \exp\left\{-\frac{\lambda^{d(6m-d)/(4m^2)} n t^2}{\kappa_K}\right\}.
\end{aligned}$$

Proof of Lemma C.2. We follow the argument used in the proof of Lemma 6.1 in [36]. Denote

$$\{Z_{n\lambda}(g)\}(\cdot) = \frac{1}{n} \sum_{i=1}^n [g(\mathbf{x}_i)K_\lambda(\mathbf{x}_i, \cdot) - \mathbb{E}_{\mathbf{x}}\{g(\mathbf{x})K_\lambda(\mathbf{x}, \cdot)\}].$$

Fix $g, h \in \mathcal{H}$, n , and λ , consider the following sequence of martingale $(X_j)_{j=0}^\infty$ in \mathcal{H} :

$$X_j = \begin{cases} 0, & \text{if } j = 0, \\ j\{Z_{j\lambda}(g) - Z_{j\lambda}(h)\}, & \text{if } j = 1, \dots, n \\ X_n, & \text{if } j \geq n+1. \end{cases}$$

Clearly, for $j = 1, \dots, n$,

$$(X_j - X_{j-1})(\cdot) = \{g(\mathbf{x}_j) - h(\mathbf{x}_j)\}K_\lambda(\mathbf{x}_j, \cdot) - \mathbb{E}_{\mathbf{x}}[\{g(\mathbf{x}_j) - h(\mathbf{x}_j)\}K_\lambda(\mathbf{x}_j, \cdot)]$$

and $X_j - X_{j-1} = 0$ for $j \geq n+1$. Observe that

$$\|K_\lambda(\mathbf{x}_j, \cdot)\|_\lambda = \sqrt{\langle K_\lambda(\mathbf{x}_j, \cdot), K_\lambda(\mathbf{x}_j, \cdot) \rangle_\lambda} = \sqrt{K_\lambda(\mathbf{x}_j, \mathbf{x}_j)} \leq C_K \lambda^{-d/(4m)}$$

with probability one. Therefore, with probability one, we have

$$\|X_j - X_{j-1}\|_\lambda^2 \leq 4C_K^2 \lambda^{-d/(2m)} \|g - h\|_{L_\infty}^2$$

for $j = 1, \dots, n$, and hence, we invoke the bounded difference inequality for martingales in Banach space (Lemma C.1) to derive

$$\begin{aligned} \mathbb{P}(\|Z_{n\lambda}(g) - Z_{n\lambda}(h)\|_\lambda \geq t) &= \mathbb{P}(\|n\{Z_{n\lambda}(g) - Z_{n\lambda}(h)\}\|_\lambda \geq nt) \\ &\leq \mathbb{P}\left(\sup_{j \geq 1} \|j\{Z_{j\lambda}(g) - Z_{j\lambda}(h)\}\|_\lambda \geq nt\right) \\ &\leq 2 \exp\left\{-\frac{nt^2}{8C_K^2 \lambda^{-d/(2m)} \|g - h\|_{L_\infty}^2}\right\}. \end{aligned}$$

Applying Lemma 8.1 in [16], we obtain the following bound

$$(C.8) \quad \|\|Z_{n\lambda}(g) - Z_{n\lambda}(h)\|_\lambda\|_{\psi_2} \leq \frac{\sqrt{24}C_K^2}{\sqrt{n}} \lambda^{-d/(4m)} \|g - h\|_{L_\infty},$$

where $\|\cdot\|_{\psi_2}$ is the Orlicz norm associated with $\psi_2(s) = \exp(s^2) - 1$.

Now let $\tau = \{\log(3/2)\}^{1/2}$ and set $\phi(x) = \psi_2(\tau x)$. Clearly, $\phi(1) = 1/2$, and $\phi(x)\phi(y) \leq \phi(xy)$ for any $x, y \geq 1$. Applying Lemma 8.2 in [16], the Orlicz norm of the maximum of finitely many random variables can be bounded by the maximum of these Orlicz norms as follows:

$$\left\|\max_{1 \leq i \leq k} (\tau \xi_i)\right\|_{\psi_2} = \left\|\max_{1 \leq i \leq k} \xi_i\right\|_\phi \leq 2\phi^{-1}(k) \max_{1 \leq i \leq k} \|\xi_i\|_\phi = \frac{2}{\tau} \psi_2^{-1}(k) \max_{1 \leq i \leq k} \|\tau \xi_i\|_{\psi_2},$$

namely,

$$(C.9) \quad \left\| \max_{1 \leq i \leq k} \xi_i \right\|_{\psi_2} \leq \frac{2}{\tau} \psi_2^{-1}(k) \max_{1 \leq i \leq k} \|\xi_i\|_{\psi_2},$$

where $\{\xi_i\}_{i=1}^k$ are finitely many random variables.

Next we apply the “chaining” argument. Let $\varepsilon > 0$ be some constant to be determined later. Construct a sequence of function classes $(\mathcal{G}_j)_{j=0}^\infty$ in $\mathcal{H}_\lambda(1)$ satisfying the following conditions:

- (i) For any \mathcal{G}_j and any $h_j, g_j \in \mathcal{G}_j$, $\|h_j - g_j\|_{L_\infty} \geq \varepsilon/2^j$, and \mathcal{G}_j is maximal in the sense that for any $g_j \notin \mathcal{G}_j$, there exists some $h_j \in \mathcal{G}_j$ such that $\|h_j - g_j\|_{L_\infty} < \varepsilon/2^j$.
- (ii) For any \mathcal{G}_{j+1} , and any $g_{j+1} \in \mathcal{G}_{j+1}$, select a unique element $g_j \in \mathcal{G}_j$ such that $\|g_{j+1} - g_j\|_{L_\infty} \leq \varepsilon/2^j$. Thus, there exists a finite sequence $(g_0, g_1, \dots, g_{j+1})$ such that $\|g_i - g_{i+1}\|_{L_\infty} \leq \varepsilon/2^i$ for $i = 0, \dots, j$, and $g_i \in \mathcal{G}_i$.

Therefore, for any $g_{j+1}, h_{j+1} \in \mathcal{G}_{j+1}$ with $\|g_{j+1} - h_{j+1}\|_{L_\infty} \leq \varepsilon$, there exists two sequences $(g_i)_{i=0}^{j+1}, (h_i)_{i=0}^{j+1}$, such that $g_i, h_i \in \mathcal{G}_i$, $\max\{\|g_i - g_{i+1}\|_{L_\infty}, \|h_i - h_{i+1}\|_{L_\infty}\} \leq \varepsilon/2^i$, and that

$$\begin{aligned} \|g_0 - h_0\|_{L_\infty} &\leq \sum_{i=0}^j (\|g_i - g_{i+1}\|_{L_\infty} + \|h_i - h_{i+1}\|_{L_\infty}) + \|h_{j+1} - g_{j+1}\|_{L_\infty} \\ &\leq 2 \sum_{i=0}^j \frac{\varepsilon}{2^i} + \varepsilon \leq 5\varepsilon, \end{aligned}$$

and hence, by (C.8) one has

$$(C.10) \quad \|\|Z_{n\lambda}(g_0) - Z_{n\lambda}(h_0)\|_\lambda\|_{\psi_2} \leq \frac{5\sqrt{24}C_K^2}{\sqrt{n}} \lambda^{-p/(4m)} \varepsilon.$$

We also notice that $\mathcal{G}_j \subset \mathcal{H}_\lambda(1) \subset \{f \in \mathcal{H} : \|f\|_{\mathcal{H}} \leq \lambda^{-1/2}\}$, and therefore, the cardinality of \mathcal{G}_j can be bounded by the metric entropy of $\{f \in \mathcal{H} : \|f\|_{\mathcal{H}} \leq \lambda^{-1/2}\}$, which is known in the literature [6]:

$$\begin{aligned} \log|\mathcal{G}_j| &\leq \log\mathcal{N}_{[\cdot]} \left(\varepsilon/2^j, \{f \in \mathcal{H} : \|f\|_{\mathcal{H}} \leq \lambda^{-1/2}\}, \|\cdot\|_{L_\infty} \right) \\ &\leq c_0 \lambda^{-p/(2m)} \left(\frac{\varepsilon}{2^j} \right)^{-p/m}, \end{aligned}$$

where c_0 is some absolute constant.

Now suppose g, h are arbitrary functions in $\mathcal{H}_\lambda(1)$ such that $\|g - h\|_{L_\infty} \leq \varepsilon/2$. For any $j \geq 2$, there exists $g_j, h_j \in \mathcal{G}_j$ such that

$$\max\{\|g_j - g\|_{L_\infty}, \|h_j - h\|_{L_\infty}\} \leq \varepsilon/2^j,$$

and hence, $\|g_j - h_j\|_{L_\infty} \leq \varepsilon$. Therefore, for any $j \geq 2$,

$$\begin{aligned} & \left\| \sup_{g, h \in \mathcal{W}_2^m(\mathcal{X}, 1), \|g-h\|_{L_\infty} \leq \varepsilon} \|Z_{n\lambda}(g) - Z_{n\lambda}(h)\|_\lambda \right\|_{\psi_2} \\ & \leq \left\| \sup_{g, h \in \mathcal{W}_2^m(\mathcal{X}, 1), \|g-h\|_{L_\infty} \leq \varepsilon} \left(\|Z_{n\lambda}(g) - Z_{n\lambda}(g_j)\|_\lambda + \|Z_{n\lambda}(g_j) - Z_{n\lambda}(h_j)\|_\lambda \right. \right. \\ & \quad \left. \left. + \|Z_{n\lambda}(h_j) - Z_{n\lambda}(h)\|_\lambda \right) \right\|_{\psi_2} \\ & \leq \frac{2\sqrt{24}C_K^2}{\sqrt{n}} \lambda^{-d/(4m)} \max\{\|g - g_j\|_{L_\infty}, \|h - h_j\|_{L_\infty}\} \\ & \quad + \left\| \sup_{g, h \in \mathcal{W}_2^m(\mathcal{X}, 1), \|g-h\|_{L_\infty} \leq \varepsilon} \|Z_{n\lambda}(g_j) - Z_{n\lambda}(h_j)\|_\lambda \right\|_{\psi_2} \\ & \leq \frac{2\sqrt{24}C_K^2}{\sqrt{n}} \frac{\lambda^{-d/(4m)} \varepsilon}{2^j} + \left\| \max_{g_j, h_j \in \mathcal{G}_j, \|g_j-h_j\|_{L_\infty} \leq \varepsilon} \|Z_{n\lambda}(g_j) - Z_{n\lambda}(h_j)\|_\lambda \right\|_{\psi_2}. \end{aligned}$$

We focus on the second term of the preceding display. Fix $j \geq 2$, for any $g_j, h_j \in \mathcal{G}_j$, consider the finite sequences (g_0, g_1, \dots, g_j) and (h_0, h_1, \dots, h_j) such that $g_i, h_i \in \mathcal{G}_i$ and $\|g_i - g_{i+1}\|_{L_\infty} \leq \varepsilon/2^i$, $i = 1, \dots, j-1$. Invoking the inequality (C.9), we have

$$\begin{aligned} & \left\| \max_{g_j, h_j \in \mathcal{G}_j, \|g_j-h_j\|_{L_\infty} \leq \varepsilon} \|Z_{n\lambda}(g_j) - Z_{n\lambda}(h_j)\|_\lambda \right\|_{\psi_2} \\ & \leq \left\| \max_{g_j, h_j \in \mathcal{G}_j, \|g_j-h_j\|_{L_\infty} \leq \varepsilon} \|\{Z_{n\lambda}(g_j) - Z_{n\lambda}(h_j)\} - \{Z_{n\lambda}(g_0) - Z_{n\lambda}(h_0)\}\|_\lambda \right\|_{\psi_2} \\ & \quad + \left\| \max_{g_0, h_0 \in \mathcal{G}_0, \|g_0-h_0\|_{L_\infty} \leq \varepsilon} \|Z_{n\lambda}(g_0) - Z_{n\lambda}(h_0)\|_\lambda \right\|_{\psi_2} \\ & \leq \left\| \max_{g_j, h_j \in \mathcal{G}_j, \|g_j-h_j\|_{L_\infty} \leq \varepsilon} \|\{Z_{n\lambda}(g_j) - Z_{n\lambda}(h_j)\} - \{Z_{n\lambda}(g_0) - Z_{n\lambda}(h_0)\}\|_\lambda \right\|_{\psi_2} \\ & \quad + \frac{2}{\tau} \sqrt{\log(1 + |\mathcal{G}_0 \times \mathcal{G}_0|)} \max_{(g_0, h_0) \in \mathcal{G}_0 \times \mathcal{G}_0, \|g_0-h_0\|_{L_\infty} \leq \varepsilon} \|Z_{n\lambda}(g_0) - Z_{n\lambda}(h_0)\|_\lambda \Big|_{\psi_2}. \end{aligned}$$

Clearly, the second term can be bounded by inequality (C.10):

$$\begin{aligned} & \frac{2}{\tau} \sqrt{\log(1 + |\mathcal{G}_0 \times \mathcal{G}_0|)} \max_{(g_0, h_0) \in \mathcal{G}_0 \times \mathcal{G}_0, \|g_j - h_j\|_{L_\infty} \leq \varepsilon} \|Z_{n\lambda}(g_0) - Z_{n\lambda}(h_0)\|_\lambda \|_{\psi_2} \\ & \leq \left(\frac{10\sqrt{24}C_K^2}{\tau} \right) \frac{\lambda^{-p/(4m)} \varepsilon}{\sqrt{n}} \sqrt{\log \{1 + \exp(2c_0 \lambda^{-p/(2m)} \varepsilon^{-p/m})\}}, \end{aligned}$$

since

$$\begin{aligned} |\mathcal{G}_0 \times \mathcal{G}_0| &= |\mathcal{G}_0|^2 \leq \exp(2 \log \mathcal{N}_{[\cdot]}(\varepsilon, \{\|f\|_\lambda \leq 1\}, \|\cdot\|_{L_\infty})) \\ (C.11) \quad &\leq \exp(2c_0 \lambda^{-p/(2m)} \varepsilon^{-p/m}), \end{aligned}$$

it suffices to bound the first term. Write

$$\begin{aligned} & \left\| \max_{g_j, h_j \in \mathcal{G}_j, \|g_j - h_j\|_{L_\infty} \leq \varepsilon} \{Z_{n\lambda}(g_j) - Z_{n\lambda}(h_j)\} - \{Z_{n\lambda}(g_0) - Z_{n\lambda}(h_0)\} \right\|_\lambda \Big\|_{\psi_2} \\ & \leq 2 \sum_{i=0}^{j-1} \left\| \max_{(g_i, g_{i+1}) \in \mathcal{G}_i \times \mathcal{G}_{i+1}, \|g_i - g_{i+1}\|_{L_\infty} \leq \varepsilon/2^i} \|Z_{n\lambda}(g_{i+1}) - Z_{n\lambda}(g_i)\|_\lambda \right\|_{\psi_2} \\ & \leq 2 \sum_{i=0}^{j-1} \frac{2}{\tau} \sqrt{\log(1 + |\mathcal{G}_i| \times |\mathcal{G}_{i+1}|)} \\ & \quad \times \max_{(g_i, g_{i+1}) \in \mathcal{G}_i \times \mathcal{G}_{i+1}, \|g_i - g_{i+1}\|_{L_\infty} \leq \varepsilon/2^i} \|Z_{n\lambda}(g_{i+1}) - Z_{n\lambda}(g_i)\|_\lambda \|_{\psi_2} \\ & \leq \frac{4\sqrt{24}C_K^2 \lambda^{-p/(4m)}}{\tau \sqrt{n}} \sum_{i=0}^{j-1} \sqrt{\log \left[1 + \exp \left\{ 2c_0 \lambda^{-p/(2m)} (\varepsilon/2^i)^{-p/m} \right\} \right]} \varepsilon/2^i, \end{aligned}$$

where inequalities (C.8) and (C.9) are applied. Bounding the sum by integral, we have

$$\begin{aligned} & \sum_{i=0}^{j-1} \sqrt{\log \left[1 + \exp \left\{ 2c_0 \lambda^{-p/(2m)} (\varepsilon/2^i)^{-p/m} \right\} \right]} \varepsilon/2^i \\ & \leq \sum_{i=0}^{j-1} \int_{\varepsilon/2^{i+1}}^{\varepsilon/2^i} \sqrt{\log \{1 + \exp(2c_0 \lambda^{-p/(2m)} x^{-p/m})\}} dx \\ & \leq \int_0^\varepsilon \sqrt{\log \{1 + \exp(2c_0 \lambda^{-p/(2m)} x^{-p/m})\}} dx. \end{aligned}$$

Putting all pieces above together, we obtain the following bound:

$$\left\| \sup_{g, h \in \mathcal{W}_2^m(\mathcal{X}, 1), \|g - h\|_{L_\infty} \leq \varepsilon} \|Z_{n\lambda}(g) - Z_{n\lambda}(h)\|_\lambda \right\|_{\psi_2}$$

$$\begin{aligned}
 &\lesssim \frac{\lambda^{-p/(4m)}}{\sqrt{n}} \left[\frac{\varepsilon}{2^j} + \int_0^\varepsilon \sqrt{\log\{1 + \exp(2c_0\lambda^{-p/(2m)}x^{-p/m})\}} dx \right. \\
 &\quad \left. + \varepsilon \sqrt{\log\{1 + \exp(2c_0\lambda^{-p/(2m)}\varepsilon^{-p/m})\}} \right].
 \end{aligned}$$

By taking $j \rightarrow \infty$, we can let the first term in the squared bracket tend to 0, and hence,

$$\begin{aligned}
 &\left\| \sup_{g, h \in \mathcal{W}_2^m(\mathcal{X}, 1), \|g-h\|_{L_\infty} \leq \varepsilon} \|Z_{n\lambda}(g) - Z_{n\lambda}(h)\|_\lambda \right\|_{\psi_2} \\
 &\lesssim \frac{\lambda^{-p/(4m)}}{\sqrt{n}} \left[\int_0^\varepsilon \sqrt{\log\{1 + \exp(2c_0\lambda^{-p/(2m)}x^{-p/m})\}} dx \right. \\
 &\quad \left. + \varepsilon \sqrt{\log\{1 + \exp(2c_0\lambda^{-p/(2m)}\varepsilon^{-p/m})\}} \right] \\
 &\lesssim \frac{\lambda^{-p/(4m)}}{\sqrt{n}} \int_0^\varepsilon \sqrt{\log\{1 + \exp(2c_0\lambda^{-p/(2m)}x^{-p/m})\}} dx.
 \end{aligned}$$

Now we take $h = 0$, which implies $Z_{n\lambda}(h) = 0$ by the construction of $Z_{n\lambda}$. Furthermore, by the property of reproducing kernel K_λ and the Cauchy-Schwarz inequality,

$$\begin{aligned}
 \|g - h\|_{L_\infty} &\leq \sup_{\mathbf{x} \in \mathcal{X}} |g(\mathbf{x})| = \sup_{\mathbf{x} \in \mathcal{X}} |\langle g(\cdot), K_\lambda(\mathbf{x}, \cdot) \rangle_\lambda| \\
 &\leq \sup_{\mathbf{x} \in \mathcal{X}} \|g\|_\lambda \sqrt{\langle K_\lambda(\mathbf{x}, \cdot), K_\lambda(\mathbf{x}, \cdot) \rangle_\lambda} \leq C_K \lambda^{-p/(4m)}.
 \end{aligned}$$

Taking $\varepsilon = C_K \lambda^{-p/(4m)}$, we obtain

$$\begin{aligned}
 &\left\| \sup_{g \in \mathcal{W}_2^m(\mathcal{X}, 1)} \|Z_{n\lambda}(g)\|_\lambda \right\|_{\psi_2} \\
 &\leq \left\| \sup_{g \in \mathcal{W}_2^m(\mathcal{X}, 1), \|g\|_{L_\infty} \leq \varepsilon} \|Z_{n\lambda}(g)\|_\lambda \right\|_{\psi_2} \\
 &\leq \left\| \sup_{g, h \in \mathcal{W}_2^m(\mathcal{X}, 1), \|g-h\|_{L_\infty} \leq \varepsilon} \|Z_{n\lambda}(g) - Z_{n\lambda}(h)\|_\lambda \right\|_{\psi_2} \\
 &\lesssim n^{-1/2} \lambda^{-p/(4m)} \int_0^\varepsilon \sqrt{\log\{1 + \exp(2c_0\lambda^{-p/(2m)}x^{-p/m})\}} dx \\
 &\lesssim n^{-1/2} \lambda^{-p(6m-p)/(8m^2)}.
 \end{aligned}$$

Hence, invoking Lemma 8.1 in [16], we finally obtain

$$\mathbb{P} \left(\sup_{g \in \mathcal{W}_2^m(\mathcal{X}, 1)} \|Z_{n\lambda}(g)\|_\lambda > t \right) \leq 2 \exp \left\{ -\frac{nt^2}{\kappa_K^2 \lambda^{-p(6m-p)/(4m^2)}} \right\},$$

for some absolute constant κ_K depending on K only, completing the proof. \square

Appendix D Proof for Section 4.2. Denote $\hat{\boldsymbol{\theta}}_z := \hat{\boldsymbol{\theta}}_{\lambda, \lambda_z, n}$, $\hat{\delta}_z(\cdot) := \hat{\delta}_{\lambda, \lambda_z, n}(\cdot)$ and $\ell_z(\boldsymbol{\theta}, \delta) := \ell_{\lambda, \lambda_z, n}(\boldsymbol{\theta}, \delta)$ in (3.7).

We need the following Corollary D.1 and Lemma D.1 to prove theorem 4.2. Corollary D.1 is a direct consequence of Theorem 4.1. We repeatedly use the fact that for any $f(\cdot) \in L_2(\mathcal{X})$, there exists a constant C_ρ such that $\|f\|_{L_2(\mathcal{X})} \leq C_\rho \|f\|_{\mathcal{H}}$ in the following proof.

COROLLARY D.1. *Denote $\hat{\delta}_{z, \boldsymbol{\theta}} = \arg \min_{\delta \in \mathcal{H}} \ell_z(\boldsymbol{\theta}, \delta)$ for each $\boldsymbol{\theta} \in \boldsymbol{\Theta}$. Under the Assumptions A1 to A6, for sufficiently large n and any $\alpha > 2$ and $C_\beta \in (0, 1)$, with probability at least $1 - \exp\{-(\alpha - 2)/3\} - \exp\{-n^{C_\beta \beta}\}$, one has*

$$\begin{aligned} & \sup_{\boldsymbol{\theta} \in \boldsymbol{\Theta}} \|\hat{\delta}_{z, \boldsymbol{\theta}}(\cdot) - (y^R(\cdot) - f^M(\cdot, \boldsymbol{\theta}))\|_{L_2(\mathcal{X})} \\ & \leq 2 \left[\sqrt{2} \left(\sup_{\boldsymbol{\theta} \in \boldsymbol{\Theta}} \|y^R(\cdot) - f^M(\cdot, \boldsymbol{\theta})\|_{L_2(\mathcal{X})} \right. \right. \\ & \quad \left. \left. + \sup_{\boldsymbol{\theta} \in \boldsymbol{\Theta}} \|y^R(\cdot) - f^M(\cdot, \boldsymbol{\theta})\|_{\mathcal{H}} \right) + C_K \sigma_0 \alpha^{1/2} \right] n^{-\frac{m}{2m+p}}, \end{aligned}$$

and

$$\begin{aligned} \sup_{\boldsymbol{\theta} \in \boldsymbol{\Theta}} \|\hat{\delta}_{z, \boldsymbol{\theta}}(\cdot)\|_{\mathcal{H}} & \leq (2\sqrt{2} + 1) \sup_{\boldsymbol{\theta} \in \boldsymbol{\Theta}} \|(y^R(\cdot) - f^M(\cdot, \boldsymbol{\theta}))\|_{\mathcal{H}} \\ & \quad + 2\sqrt{2} \sup_{\boldsymbol{\theta} \in \boldsymbol{\Theta}} \|y^R(\cdot) - f^M(\cdot, \boldsymbol{\theta})\|_{L_2(\mathcal{X})} + 2\sqrt{2} C_K \sigma_0 \alpha^{1/2} \end{aligned}$$

by choosing $\lambda = n^{-2m/(2m+p)}$ and $\lambda_z = \lambda^{-1/2}$, where C_K is a constant depending on the kernel $K(\cdot, \cdot)$.

LEMMA D.1. *Under assumptions A1 to A6,*

(i) *it holds that*

$$\sup_{\boldsymbol{\theta} \in \boldsymbol{\Theta}} \left| \frac{1}{n} \sum_{i=1}^n (y^R(\mathbf{x}_i) - f^M(\mathbf{x}_i, \boldsymbol{\theta}) - \hat{\delta}_{z, \boldsymbol{\theta}}(\mathbf{x}_i))^2 \right|$$

$$\left| - \int_{\mathbf{x} \in \mathcal{X}} (y^R(\mathbf{x}) - f^M(\mathbf{x}, \boldsymbol{\theta}) - \hat{\delta}_{z, \boldsymbol{\theta}}(\mathbf{x}))^2 d\mathbf{x} \right| = o_p(n^{-1/2}),$$

and

$$\sup_{\boldsymbol{\theta} \in \boldsymbol{\Theta}} \left| \frac{1}{n} \sum_{i=1}^n (y^R(\mathbf{x}_i) - f^M(\mathbf{x}_i, \boldsymbol{\theta}) - \hat{\delta}_{z, \boldsymbol{\theta}}(\mathbf{x}_i)) \epsilon_i \right| = o_p(n^{-1/2});$$

(ii) for any $j = 1, \dots, q$, one has

$$\begin{aligned} & \frac{1}{n} \sum_{i=1}^n (y^R(\mathbf{x}_i) - f^M(\mathbf{x}_i, \hat{\boldsymbol{\theta}}_z) - \hat{\delta}_z(\mathbf{x}_i)) \frac{\partial f^M(\mathbf{x}_i, \hat{\boldsymbol{\theta}}_z)}{\partial \theta_j} \\ &= \int_{\mathbf{x} \in \mathcal{X}} (y^R(\mathbf{x}) - f^M(\mathbf{x}, \hat{\boldsymbol{\theta}}_z) - \hat{\delta}_z(\mathbf{x})) \frac{\partial f^M(\mathbf{x}, \hat{\boldsymbol{\theta}}_z)}{\partial \theta_j} d\mathbf{x} + o_p(n^{-1/2}). \end{aligned}$$

PROOF. Denote

$$\mathcal{W}_2^m(\mathcal{H}, B) := \left\{ f(\cdot) = \sum_{j=1}^{\infty} f_j \phi(\cdot) \in L_2(\mathcal{X}) : \sum_{j=1}^{\infty} j^{2m/p} f_j^2 \leq B^2 \right\},$$

and

$$\begin{aligned} s_i^2(\boldsymbol{\theta}, \delta) &:= (y^R(\mathbf{x}_i) - f^M(\mathbf{x}_i, \boldsymbol{\theta}) - \delta(\mathbf{x}_i))^2, \\ u_i(\boldsymbol{\theta}, \delta) &:= (y^R(\mathbf{x}_i) - f^M(\mathbf{x}_i, \boldsymbol{\theta}) - \delta(\mathbf{x}_i)) \epsilon_i, \\ r_i^2(\boldsymbol{\theta}, \delta) &:= (y^R(\mathbf{x}_i) - f^M(\mathbf{x}_i, \boldsymbol{\theta}) - \delta(\mathbf{x}_i)) \frac{\partial f^M(\mathbf{x}, \boldsymbol{\theta})}{\partial \theta_j} \end{aligned}$$

for $(\boldsymbol{\theta}, \delta) \in \boldsymbol{\Theta} \times \mathcal{W}_2^m(\mathcal{X}, B)$ and some $B > 0$ that will be specified later. Define the empirical processes

$$\begin{aligned} \bar{s}^2(\boldsymbol{\theta}, \delta) &:= \frac{1}{\sqrt{n}} \sum_{i=1}^n \{s_i^2(\delta, \boldsymbol{\theta}) - \mathbb{E}_{\mathbf{x}_i}[s_i^2(\delta, \boldsymbol{\theta})]\}, \\ \bar{u}(\boldsymbol{\theta}, \delta) &:= \frac{1}{\sqrt{n}} \sum_{i=1}^n \{u_i(\delta, \boldsymbol{\theta}) - \mathbb{E}_{\mathbf{x}_i, \epsilon_i}[u_i(\delta, \boldsymbol{\theta})]\}, \\ \bar{r}(\boldsymbol{\theta}, \delta) &:= \frac{1}{\sqrt{n}} \sum_{i=1}^n \{r_i(\delta, \boldsymbol{\theta}) - \mathbb{E}_{\mathbf{x}_i}[r_i(\delta, \boldsymbol{\theta})]\}, \end{aligned}$$

where

$$\mathbb{E}_{\mathbf{x}_i}[s_i^2(\boldsymbol{\theta}, \delta)] = \int_{\mathbf{x} \in \mathcal{X}} (y^R(\mathbf{x}) - f^M(\mathbf{x}, \boldsymbol{\theta}) - \delta(\mathbf{x}))^2 d\mathbf{x},$$

$$\begin{aligned}\mathbb{E}_{\mathbf{x}_i, \epsilon_i}[u_i(\boldsymbol{\theta}, \delta)] &= \int_{\mathbf{x} \in \mathcal{X}} (y^R(\mathbf{x}) - f^M(\mathbf{x}, \boldsymbol{\theta}) - \delta(\mathbf{x})) \epsilon_i d\mathbf{x} = 0, \\ \mathbb{E}_{\mathbf{x}_i}[r_i(\boldsymbol{\theta}, \delta)] &= \int_{\mathbf{x} \in \mathcal{X}} (y^R(\mathbf{x}) - f^M(\mathbf{x}, \boldsymbol{\theta}) - \delta(\mathbf{x})) \frac{\partial f^M(\mathbf{x}, \boldsymbol{\theta})}{\partial \theta_j} d\mathbf{x}.\end{aligned}$$

By Assumptions A3 and A4, the function classes $\{\partial f^M(\cdot, \boldsymbol{\theta})/\partial \theta_j : \boldsymbol{\theta} \in \boldsymbol{\Theta}\}$ and $\mathcal{F} = \{y^R(\cdot) - f^M(\cdot, \boldsymbol{\theta}), \boldsymbol{\theta} \in \boldsymbol{\Theta}\}$ are Donsker. Note that, by definition, $\mathcal{W}_2^m(\mathcal{X}, B)$ is also Donsker. Since both $\mathcal{W}_2^m(\mathcal{X}, B)$ and \mathcal{F} are uniformly bounded, the function classes

$$\begin{aligned}&\{(y^R(\cdot) - f^M(\cdot, \boldsymbol{\theta}) - \delta(\cdot))^2 : \boldsymbol{\theta} \in \boldsymbol{\Theta}, \delta \in \mathcal{W}_2^m(\mathcal{X}, B)\}, \quad \text{and} \\ &\left\{(y^R(\cdot) - f^M(\cdot, \boldsymbol{\theta}) - \delta(\cdot)) \frac{\partial f^M(\cdot, \boldsymbol{\theta})}{\partial \theta_j} : \boldsymbol{\theta} \in \boldsymbol{\Theta}, \delta \in \mathcal{W}_2^m(\mathcal{X}, B)\right\}\end{aligned}$$

are also Donsker classes. Furthermore, letting $f_{\boldsymbol{\theta}, \delta}(\epsilon, \mathbf{x}) = (y^R(\mathbf{x}) - f^M(\mathbf{x}, \boldsymbol{\theta}) - \delta(\mathbf{x}))\epsilon$, observe that for any $(\boldsymbol{\theta}_1, \delta_1)$ and $(\boldsymbol{\theta}_2, \delta_2)$, the distance

$$\begin{aligned}&\{\mathbb{E}_0[(f_{\boldsymbol{\theta}_1, \delta_1} - f_{\boldsymbol{\theta}_2, \delta_2})^2]\}^{1/2} \\ &= \sigma_0 \|f^M(\cdot, \boldsymbol{\theta}_1) - \delta_1(\cdot) - f^M(\cdot, \boldsymbol{\theta}_2) + \delta_2(\cdot)\|_{L_2(\mathcal{X})} \\ &\leq \sigma_0 [\|f^M(\cdot, \boldsymbol{\theta}_1) - f^M(\cdot, \boldsymbol{\theta}_2)\|_{L_2(\mathcal{X})} + \|\delta_1(\cdot) - \delta_2(\cdot)\|_{L_2(\mathcal{X})}]\end{aligned}$$

can be bounded by the $L_2(\mathcal{X})$ -distance of functions in $\{f^M(\cdot, \boldsymbol{\theta}) : \boldsymbol{\theta} \in \boldsymbol{\Theta}\}$ and $\delta(\cdot) \in \mathcal{W}_2^m(\mathcal{X}, B)$. In addition, by Assumption A4 $\{f^M(\cdot, \boldsymbol{\theta}) : \boldsymbol{\theta} \in \boldsymbol{\Theta}\}$ and $\mathcal{W}_2^m(\mathcal{X}, B)$ are Donsker classes, it follows that the function class

$$\{f_{\boldsymbol{\theta}, \delta} \in C(\mathbb{R} \times \mathcal{X}) : \boldsymbol{\theta} \in \boldsymbol{\Theta}, \delta \in \mathcal{W}_2^m(\mathcal{X}, B)\}$$

is also Donsker, since its metric entropy can be upper bounded by those of $\{f^M(\cdot, \boldsymbol{\theta}) : \boldsymbol{\theta} \in \boldsymbol{\Theta}\}$ and $\mathcal{W}_2^m(\mathcal{X}, B)$. By Theorem 2.4 in [17], for any $t_1 > 0$ and any $B > 0$, there exists $t_2, t'_2, t''_2 > 0$ such that

(D.1)

$$\limsup_{n \rightarrow \infty} P \left(\sup_{\|\delta\|_{\mathcal{H}} \leq B, \boldsymbol{\theta} \in \boldsymbol{\Theta}, \|y^R(\cdot) - f^M(\cdot, \boldsymbol{\theta}) - \delta(\cdot)\|_{L_2(\mathcal{X})} \leq t_2} |\bar{s}^2(\boldsymbol{\theta}, \delta)| > t_1 \right) < t_1,$$

(D.2)

$$\limsup_{n \rightarrow \infty} P \left(\sup_{\|\delta\|_{\mathcal{H}} \leq B, \boldsymbol{\theta} \in \boldsymbol{\Theta}, \|y^R(\cdot) - f^M(\cdot, \boldsymbol{\theta}) - \delta(\cdot)\|_{L_2(\mathcal{X})} \leq t'_2} |\bar{r}(\boldsymbol{\theta}, \delta)| > t_1 \right) < t_1,$$

(D.3)

$$\limsup_{n \rightarrow \infty} P \left(\sup_{\|\delta\|_{\mathcal{H}} \leq B, \boldsymbol{\theta} \in \boldsymbol{\Theta}, \|y^R(\cdot) - f^M(\cdot, \boldsymbol{\theta}) - \delta(\cdot)\|_{L_2(\mathcal{X})} \leq t''_2} |\bar{u}(\boldsymbol{\theta}, \delta)| > t_1 \right) < t_1.$$

Note that by Corollary D.1, $\sup_{\boldsymbol{\theta} \in \Theta} \|\hat{\delta}_{z,\boldsymbol{\theta}}\|_{\mathcal{H}}$ is asymptotically tight, and therefore for any $\varepsilon > 0$, there exists $B_0 > 0$ and some integer $N \in \mathbb{N}_+$, both depending on ε , such that $P(\sup_{\boldsymbol{\theta} \in \Theta} \|\hat{\delta}_{z,\boldsymbol{\theta}}\|_{\mathcal{H}} > B_0) \leq \varepsilon/3$ for all $n > N$. Now take $B = B_0$, $t_1 = \varepsilon/3$. Then we can choose t_2 to be a value that satisfies (D.1), t'_2 satisfying (D.2), and t''_2 satisfying (D.3). By Corollary D.1 and Assumption A5, $\sup_{\boldsymbol{\theta}} \|\hat{\delta}_{z,\boldsymbol{\theta}}(\cdot) - (y^R(\cdot) - f^M(\cdot, \boldsymbol{\theta}))\|_{L_2(\mathcal{X})} = O_P(n^{-2m/(2m+p)})$, and hence there exists $t_3 > 0$, depending on ε and n , such that for all $n > N$, it holds that

$$P\left(\sup_{\boldsymbol{\theta} \in \Theta} \|y^R(\cdot) - f^M(\cdot, \boldsymbol{\theta}) - \hat{\delta}_{z,\boldsymbol{\theta}}(\cdot)\|_{L_2(\mathcal{X})} \geq t_3\right) < \varepsilon/3.$$

Without loss of generality, we may require $t_3 \leq \min\{t_2, t'_2, t''_2\}$ by taking sufficiently large n . Then for sufficiently large n , we obtain

$$\begin{aligned} & P\left(\sup_{\boldsymbol{\theta} \in \Theta} |\bar{s}^2(\boldsymbol{\theta}, \hat{\delta}_{z,\boldsymbol{\theta}})| > \varepsilon\right) \\ & \leq P\left(\sup_{\substack{\sup_{\boldsymbol{\theta}} \|\hat{\delta}_{z,\boldsymbol{\theta}}\|_{\mathcal{H}} \leq B_0, \boldsymbol{\theta} \in \Theta, \|y^R(\cdot) - f^M(\cdot, \boldsymbol{\theta}) - \hat{\delta}_{z,\boldsymbol{\theta}}(\cdot)\|_{L_2(\mathcal{X})} \leq t_2}} |\bar{s}^2(\boldsymbol{\theta}, \hat{\delta}_{z,\boldsymbol{\theta}})| > t_1\right) \\ & \quad + P\left(\sup_{\boldsymbol{\theta} \in \Theta} \|y^R(\cdot) - f^M(\cdot, \boldsymbol{\theta}) - \hat{\delta}_{z,\boldsymbol{\theta}}(\cdot)\|_{L_2(\mathcal{X})} > t_2\right) \\ & \quad + P\left(\sup_{\boldsymbol{\theta} \in \Theta} \|\hat{\delta}_{z,\boldsymbol{\theta}}\|_{\mathcal{H}} > B_0\right) \\ & < \varepsilon/3 + \varepsilon/3 + \varepsilon/3 = \varepsilon, \end{aligned}$$

and similarly,

$$P\left(\sup_{\boldsymbol{\theta} \in \Theta} |\bar{r}(\boldsymbol{\theta}, \hat{\delta}_{z,\boldsymbol{\theta}})| > \varepsilon\right) < \varepsilon \quad \text{and} \quad P\left(\sup_{\boldsymbol{\theta} \in \Theta} |\bar{u}(\boldsymbol{\theta}, \hat{\delta}_{z,\boldsymbol{\theta}})| > \varepsilon\right) < \varepsilon.$$

Therefore,

$$\begin{aligned} & \frac{1}{\sqrt{n}} \sup_{\boldsymbol{\theta} \in \Theta} |\bar{s}(\boldsymbol{\theta}, \hat{\delta}_{z,\boldsymbol{\theta}})| \\ & = \sup_{\boldsymbol{\theta} \in \Theta} \left| \frac{1}{n} \sum_{i=1}^n (y^R(\mathbf{x}_i) - f^M(\mathbf{x}_i, \boldsymbol{\theta}) - \hat{\delta}_{z,\boldsymbol{\theta}}(\mathbf{x}_i))^2 \right. \\ & \quad \left. - \int_{\mathbf{x} \in \mathcal{X}} (y^R(\mathbf{x}) - f^M(\mathbf{x}, \boldsymbol{\theta}) - \hat{\delta}_{z,\boldsymbol{\theta}}(\mathbf{x}))^2 d\mathbf{x} \right| = o_p(n^{-1/2}), \end{aligned}$$

and

$$\frac{1}{\sqrt{n}} \sup_{\boldsymbol{\theta} \in \Theta} |\bar{u}(\boldsymbol{\theta}, \hat{\delta}_{z,\boldsymbol{\theta}})| = \sup_{\boldsymbol{\theta} \in \Theta} \left| \frac{1}{n} \sum_{i=1}^n (y^R(\mathbf{x}_i) - f^M(\mathbf{x}_i, \boldsymbol{\theta}) - \hat{\delta}_{z,\boldsymbol{\theta}}(\mathbf{x}_i)) \epsilon_i \right| = o_p(n^{-1/2}),$$

completing the proof of (i). The proof of (ii) can be completed by observing that

$$\begin{aligned} & \left| \frac{1}{n} \sum_{i=1}^n (y^R(\mathbf{x}_i) - f^M(\mathbf{x}_i, \hat{\boldsymbol{\theta}}_z) - \hat{\delta}_z(\mathbf{x}_i)) \frac{\partial f^M(\mathbf{x}_i, \hat{\boldsymbol{\theta}}_z)}{\partial \theta_j} \right. \\ & \quad \left. - \int_{\mathbf{x} \in \mathcal{X}} (y^R(\mathbf{x}) - f^M(\mathbf{x}, \hat{\boldsymbol{\theta}}_z) - \hat{\delta}_z(\mathbf{x})) \frac{\partial f^M(\mathbf{x}, \hat{\boldsymbol{\theta}}_z)}{\partial \theta_j} d\mathbf{x} \right| \\ & = \frac{1}{\sqrt{n}} |\bar{r}(\hat{\boldsymbol{\theta}}_z, \hat{\delta}_{z, \hat{\boldsymbol{\theta}}_z})| \leq \frac{1}{\sqrt{n}} \sup_{\boldsymbol{\theta} \in \boldsymbol{\Theta}} |\bar{r}(\boldsymbol{\theta}, \hat{\delta}_{z, \boldsymbol{\theta}})| = o_p(n^{-1/2}). \end{aligned}$$

□

PROOF FOR THEOREM 4.2. Without loss of generality, it suffices to prove the case when $\lambda_z = \lambda^{-1/2}$. For the general case when $\lambda_z = O(\lambda^{-1/2})$, the proof follows similarly. We first show $\hat{\boldsymbol{\theta}}_z \rightarrow^p \boldsymbol{\theta}_{L_2}$. By the definition of $\hat{\boldsymbol{\theta}}_z$, $\boldsymbol{\theta}_{L_2}$, and the theory of M-estimators (see, Theorem 5.7 in [29]), it suffices to show that $\lambda^{-1/2}(\ell_z(\boldsymbol{\theta}, \hat{\delta}_{z, \boldsymbol{\theta}}) - \sigma_0^2) \rightarrow^p \|y^R(\cdot) - f^M(\cdot, \boldsymbol{\theta})\|_{L_2(\mathcal{X})}^2$ uniformly for each $\boldsymbol{\theta} \in \boldsymbol{\Theta}$. Note that

$$\begin{aligned} & \ell_z(\hat{\delta}_{z, \boldsymbol{\theta}}(\cdot), \boldsymbol{\theta}) \\ & = \frac{1}{n} \sum_{i=1}^n (y^R(\mathbf{x}_i) - f^M(\mathbf{x}_i, \boldsymbol{\theta}) - \hat{\delta}_{z, \boldsymbol{\theta}}(\mathbf{x}_i))^2 + \frac{1}{n} \sum_{i=1}^n \epsilon_i^2 \\ & \quad + \frac{2}{n} \sum_{i=1}^n (y^R(\mathbf{x}_i) - f^M(\mathbf{x}_i, \boldsymbol{\theta}) - \hat{\delta}_{z, \boldsymbol{\theta}}(\mathbf{x}_i)) \epsilon_i + \lambda \|\hat{\delta}_{z, \boldsymbol{\theta}}\|_{\mathcal{H}}^2 + \sqrt{\lambda} \|\hat{\delta}_{z, \boldsymbol{\theta}}\|_{L_2(\mathcal{X})}^2 \\ & := A_n + B_n + C_n + D_n + E_n. \end{aligned}$$

For A_n , by Lemma D.1 (i) and Corollary (D.1), one has

$$(D.4) \quad \sup_{\boldsymbol{\theta} \in \boldsymbol{\Theta}} \left| \frac{1}{n} \sum_{i=1}^n (y^R(\mathbf{x}_i) - f^M(\mathbf{x}_i, \boldsymbol{\theta}) - \hat{\delta}_{z, \boldsymbol{\theta}}(\mathbf{x}_i))^2 \right| = o_p(n^{-1/2})$$

Since $\mathbb{E}[B_n] = \sigma_0^2$ and $\mathbb{V}[B_n] = O(n^{-1})$, Chebyshev's inequality implies $(1/n) \sum_{i=1}^n \epsilon_i^2 = \sigma_0^2 + O_p(n^{-1/2})$ for B_n . For C_n , Lemma D.1 (i) guarantees that

$$\sup_{\boldsymbol{\theta} \in \boldsymbol{\Theta}} \frac{2}{n} \sum_{i=1}^n (y^R(\mathbf{x}_i) - f^M(\mathbf{x}_i, \boldsymbol{\theta}) - \hat{\delta}_{z, \boldsymbol{\theta}}(\mathbf{x}_i)) \epsilon_i = o_p(n^{-1/2})$$

Since $\lambda = O(n^{-2m/(2m+p)})$, by the asymptotic tightness of $\sup_{\boldsymbol{\theta}} \|\hat{\delta}_{z,\boldsymbol{\theta}}\|_{\mathcal{H}}$ (Corollary D.1), one has $\sup_{\boldsymbol{\theta} \in \Theta} \lambda \|\hat{\delta}_{z,\boldsymbol{\theta}}\|_{\mathcal{H}}^2 = o_p(n^{-1/2})$. By putting the above all pieces together, we obtain

$$(D.5) \quad \sup_{\boldsymbol{\theta} \in \Theta} \left| \lambda^{-1/2} (\ell_z(\hat{\delta}_{z,\boldsymbol{\theta}}(\cdot), \boldsymbol{\theta}) - \sigma_0^2) - \|\hat{\delta}_{z,\boldsymbol{\theta}}\|_{L_2(\mathcal{X})}^2 \right| = O_p((\lambda n)^{-1/2}).$$

For any $\boldsymbol{\theta}$, by the Cauchy-Schwarz inequality, one has

$$\begin{aligned} & \left| \|\hat{\delta}_{z,\boldsymbol{\theta}}\|_{L_2(\mathcal{X})}^2 - \|y^R(\cdot) - f^M(\cdot, \boldsymbol{\theta})\|_{L_2(\mathcal{X})}^2 \right| \\ & \leq \|(\hat{\delta}_{z,\boldsymbol{\theta}}(\cdot) - (y^R(\cdot) - f^M(\cdot, \boldsymbol{\theta})))\|_{L_2(\mathcal{X})} \|\hat{\delta}_{z,\boldsymbol{\theta}}(\cdot) + y^R(\cdot) - f^M(\cdot, \boldsymbol{\theta})\|_{L_2(\mathcal{X})} \end{aligned}$$

Recall that

$$\sup_{\boldsymbol{\theta} \in \Theta} \|(\hat{\delta}_{z,\boldsymbol{\theta}}(\cdot) - (y^R(\cdot) - f^M(\cdot, \boldsymbol{\theta})))\|_{L_2(\mathcal{X})} = O_p(n^{-m/(2m+d)})$$

by Corollary D.1 and Assumption A4. Using Assumptions A4 and the asymptotic tightness of $\sup_{\boldsymbol{\theta}} \|\hat{\delta}_{z,\boldsymbol{\theta}}\|_{\mathcal{H}}$ (Corollary D.1), one has

$$\begin{aligned} & \|\hat{\delta}_{z,\boldsymbol{\theta}}(\cdot) + y^R(\cdot) - f^M(\cdot, \boldsymbol{\theta})\|_{L_2(\mathcal{X})} \\ & \leq \|\hat{\delta}_{z,\boldsymbol{\theta}}(\cdot)\|_{L_2(\mathcal{X})} + \sup_{\boldsymbol{\theta} \in \Theta} \|y^R(\cdot) - f^M(\cdot, \boldsymbol{\theta})\|_{L_2(\mathcal{X})} \\ & \leq C_\rho \|\hat{\delta}_{z,\boldsymbol{\theta}}(\cdot)\|_{\mathcal{H}} + \sup_{\boldsymbol{\theta} \in \Theta} \|y^R(\cdot) - f^M(\cdot, \boldsymbol{\theta})\|_{\mathcal{H}} = O_p(1). \end{aligned}$$

Thus

$$\sup_{\boldsymbol{\theta} \in \Theta} \left| \|\hat{\delta}_{z,\boldsymbol{\theta}}\|_{L_2(\mathcal{X})}^2 - \|y^R(\cdot) - f^M(\cdot, \boldsymbol{\theta})\|_{L_2(\mathcal{X})}^2 \right| = O_p(n^{-m/(2m+d)}),$$

and hence,

$$\sup_{\boldsymbol{\theta} \in \Theta} \left| \lambda^{-1/2} (\ell_z(\boldsymbol{\theta}, \hat{\delta}_{z,\boldsymbol{\theta}}) - \sigma_0^2) - \|y^R(\cdot) - f^M(\cdot, \boldsymbol{\theta})\|_{L_2(\mathcal{X})}^2 \right| = o_p(1),$$

from which we conclude $\hat{\boldsymbol{\theta}}_z \rightarrow^p \boldsymbol{\theta}_{L_2}$.

Next we derive the convergence rate of $\hat{\boldsymbol{\theta}}_z$. Apply the Fréchet derivative on ℓ_z with regard to $\delta(\cdot)$ and the partial derivative on ℓ_z with regard to θ_j , $j = 1, \dots, q$. For any $g(\cdot) \in \mathcal{H}$, $\hat{\delta}_z$ and $\hat{\boldsymbol{\theta}}_z$ satisfy

$$\begin{aligned} 0 &= -\frac{2}{n} \sum_{i=1}^n (y_i^F - f(\mathbf{x}_i, \hat{\boldsymbol{\theta}}_z) - \hat{\delta}_z(\mathbf{x}_i)) g(\mathbf{x}_i) + 2\lambda \langle \hat{\delta}_z(\cdot), g(\cdot) \rangle_{\mathcal{H}} \\ (D.6) \quad &+ 2\sqrt{\lambda} \langle \hat{\delta}_z(\cdot), g(\cdot) \rangle_{L_2(\mathcal{X})}, \end{aligned}$$

$$(D.7) \quad 0 = -\frac{2}{n} \sum_{i=1}^n (y_i^F - f(\mathbf{x}_i, \hat{\boldsymbol{\theta}}_z) - \hat{\delta}_z(\mathbf{x}_i)) \frac{\partial f^M(\mathbf{x}_i, \hat{\boldsymbol{\theta}}_z)}{\partial \theta_j}.$$

Choosing $g(\cdot) = \frac{\partial f^M(\cdot, \hat{\boldsymbol{\theta}}_z)}{\partial \theta_j}$ and plugging (D.7) into (D.6), one has

$$(D.8) \quad \sqrt{\lambda} \left\langle \hat{\delta}_z(\cdot), \frac{\partial f^M(\cdot, \hat{\boldsymbol{\theta}}_z)}{\partial \theta_j} \right\rangle_{\mathcal{H}} + \left\langle \hat{\delta}_z(\cdot), \frac{\partial f^M(\cdot, \hat{\boldsymbol{\theta}}_z)}{\partial \theta_j} \right\rangle_{L_2(\mathcal{X})} = 0.$$

Substituting (D.7) into (D.8) and by Lemma D.1 (ii), we have

$$\begin{aligned} 0 &= -\frac{1}{n} \sum_{i=1}^n (y_i^F - f(\mathbf{x}_i, \hat{\boldsymbol{\theta}}_z) - \hat{\delta}_z(\mathbf{x}_i)) \frac{\partial f^M(\mathbf{x}_i, \hat{\boldsymbol{\theta}}_z)}{\partial \theta_j} \\ &= -\int (y^R(\mathbf{x}) - f^M(\mathbf{x}, \hat{\boldsymbol{\theta}}_z)) \frac{\partial f^M(\mathbf{x}, \hat{\boldsymbol{\theta}}_z)}{\partial \theta_j} d\mathbf{x} + \left\langle \hat{\delta}_z(\cdot), \frac{\partial f^M(\cdot, \hat{\boldsymbol{\theta}}_z)}{\partial \theta_j} \right\rangle_{L_2(\mathcal{X})} \\ &\quad - \frac{1}{n} \sum_{i=1}^n \epsilon_i \frac{\partial f^M(\mathbf{x}_i, \hat{\boldsymbol{\theta}}_z)}{\partial \theta_j} + o_p(n^{-1/2}) \\ &= \int \frac{\partial (y^R(\mathbf{x}) - f^M(\mathbf{x}, \hat{\boldsymbol{\theta}}_z))^2}{\partial \theta_j} d\mathbf{x} - \sqrt{\lambda} \left\langle \hat{\delta}_z(\cdot), \frac{\partial f^M(\cdot, \hat{\boldsymbol{\theta}}_z)}{\partial \theta_j} \right\rangle_{\mathcal{H}} \\ &\quad - \frac{1}{n} \sum_{i=1}^n \epsilon_i \frac{\partial f^M(\mathbf{x}_i, \hat{\boldsymbol{\theta}}_z)}{\partial \theta_j} + o_p(n^{-1/2}). \end{aligned}$$

Applying Taylor expansion to the first term on the right-hand side at $\boldsymbol{\theta}_{L_2}$, for any $j = 1, \dots, q$, we obtain

$$\begin{aligned} &\left\{ \int \frac{\partial^2 (y^R(\mathbf{x}) - f^M(\mathbf{x}, \tilde{\boldsymbol{\theta}}_z))^2}{\partial \theta_j \partial \boldsymbol{\theta}} d\mathbf{x} \right\}^T (\hat{\boldsymbol{\theta}}_z - \boldsymbol{\theta}_{L_2}) \\ &= \left\{ \int \frac{\partial^2 (y^R(\mathbf{x}) - f^M(\mathbf{x}, \boldsymbol{\theta}_{L_2}))^2}{\partial \theta_j \partial \boldsymbol{\theta}} d\mathbf{x} + o_p(1) \right\}^T (\hat{\boldsymbol{\theta}}_z - \boldsymbol{\theta}_{L_2}) \\ (D.9) \quad &= \sqrt{\lambda} \left\langle \hat{\delta}_z(\cdot), \frac{\partial f^M(\cdot, \hat{\boldsymbol{\theta}}_z)}{\partial \theta_j} \right\rangle_{\mathcal{H}} + \frac{1}{n} \sum_{i=1}^n \epsilon_i \frac{\partial f^M(\mathbf{x}_i, \hat{\boldsymbol{\theta}}_z)}{\partial \theta_j} + o_p(n^{-1/2}), \end{aligned}$$

where $\tilde{\boldsymbol{\theta}}_z$ lies within the q dimensional rectangle between $\boldsymbol{\theta}_{L_2}$ and $\hat{\boldsymbol{\theta}}_z$. Observe that Corollary D.1 and assumption A3 imply

$$\left| \left\langle \hat{\delta}_z, \frac{\partial f^M(\cdot, \hat{\boldsymbol{\theta}}_z)}{\partial \theta_j} \right\rangle_{\mathcal{H}} \right| \leq \|\hat{\delta}_z\|_{\mathcal{H}} \left\| \frac{\partial f^M(\cdot, \boldsymbol{\theta}_{L_2})}{\partial \theta_j} + o_p(1) \right\|_{\mathcal{H}} = O_p(1).$$

Now we consider the second term. Define the empirical process

$$G_n(\boldsymbol{\theta}) = \frac{1}{\sqrt{n}} \sum_{i=1}^n \left[\epsilon_i \frac{\partial f^M(\mathbf{x}_i, \boldsymbol{\theta})}{\partial \theta_j} - \epsilon_i \frac{\partial f^M(\mathbf{x}_i, \boldsymbol{\theta}_{L_2})}{\partial \theta_j} \right].$$

and denote

$$f_{\boldsymbol{\theta}}(\epsilon, \mathbf{x}) = \epsilon \frac{\partial f^M(\mathbf{x}, \boldsymbol{\theta})}{\partial \theta_j} - \epsilon \frac{\partial f^M(\mathbf{x}, \boldsymbol{\theta}_{L_2})}{\partial \theta_j}.$$

Since

$$\begin{aligned} \mathbb{E}_{\epsilon, \mathbf{x}} \{ [f_{\boldsymbol{\theta}_1}(\epsilon, \mathbf{x}) - f_{\boldsymbol{\theta}_2}(\epsilon, \mathbf{x})]^2 \} &= \mathbb{E}_{\epsilon, \mathbf{x}} \left[\epsilon^2 \left(\frac{\partial f^M(\mathbf{x}, \boldsymbol{\theta}_1)}{\partial \theta_j} - \frac{\partial f^M(\mathbf{x}, \boldsymbol{\theta}_2)}{\partial \theta_j} \right)^2 \right] \\ &= \sigma_0^2 \left\| \frac{\partial f^M(\mathbf{x}, \boldsymbol{\theta}_1)}{\partial \theta_j} - \frac{\partial f^M(\mathbf{x}, \boldsymbol{\theta}_2)}{\partial \theta_j} \right\|_{L_2(\mathcal{X})}^2, \end{aligned}$$

therefore the function class $\{f_{\boldsymbol{\theta}}(\epsilon, \mathbf{x}) \in C(\mathbb{R} \times \mathcal{X}) : \boldsymbol{\theta} \in \boldsymbol{\Theta}\}$ is Donsker by Assumption A3, and hence, $G_n(\boldsymbol{\theta})$ converges weakly to a tight Gaussian process, denoted by $G(\cdot)$. W.l.o.g., we may take $G(\cdot)$ a version that has uniformly continuous sample paths (see Chapter 6 in [28]). Since $G_n(\boldsymbol{\theta}_{L_2}) = 0$ for all n , it follows that $G(\boldsymbol{\theta}_{L_2}) = 0$. By the consistency of $\hat{\boldsymbol{\theta}}_z$ and the continuous mapping theorem [29], $G_n(\hat{\boldsymbol{\theta}}_z) = G(\boldsymbol{\theta}_{L_2}) + o_p(1) = o_p(1)$. Therefore,

$$\frac{1}{n} \sum_{i=1}^n \epsilon_i \frac{\partial f^M(\mathbf{x}_i, \hat{\boldsymbol{\theta}}_z)}{\partial \theta_j} = \frac{1}{\sqrt{n}} G_n(\hat{\boldsymbol{\theta}}_z) + \frac{1}{n} \sum_{i=1}^n \epsilon_i \frac{\partial f^M(\mathbf{x}_i, \boldsymbol{\theta}_{L_2})}{\partial \theta_j} = O_p(n^{-1/2})$$

To sum up,

$$\begin{aligned} &\left\{ \int \frac{\partial^2 (y^R(\mathbf{x}) - f^M(\mathbf{x}, \boldsymbol{\theta}_{L_2}))^2}{\partial \boldsymbol{\theta} \partial \boldsymbol{\theta}^T} d\mathbf{x} + o_p(1) \right\} (\hat{\boldsymbol{\theta}}_z - \boldsymbol{\theta}_{L_2}) \\ &= O_p(n^{-m/(2m+p)}) + O_p(n^{-1/2}) + o_p(n^{-1/2}) = O_p(n^{-m/(2m+p)}), \end{aligned}$$

completing the proof. \square

Appendix E Proof for Section 5. The identities in the Lemma E.1 are used repeatedly in the proof of the Theorem 5.1 and Lemma 5.1.

LEMMA E.1. Denote $\sigma^2 \mathbf{R}_{z_d}$ the covariance matrix of $(\delta_{z_d}(\mathbf{x}_1), \dots, \delta_{z_d}(\mathbf{x}_n))^T$, where the (i, j) entry being $\sigma^2 K_{z_d}(\mathbf{x}_i, \mathbf{x}_j)$ defined in (5.2). Denote $r_{z_d}(\mathbf{x}) = (K_{z_d}(\mathbf{x}, \mathbf{x}_1), \dots, K_{z_d}(\mathbf{x}, \mathbf{x}_n))^T$ for any $\mathbf{x} \in \mathcal{X}$. One has the following identities

$$(E.1) \quad \mathbf{R}_{z_d}^{-1} = \mathbf{R}^{-1} + \frac{\lambda_z}{n} \mathbf{I}_n,$$

$$(E.2) \quad \mathbf{r}_{z_d}^T(\mathbf{x}) = \frac{n}{\lambda_z} \mathbf{r}^T(\mathbf{x}) \tilde{\mathbf{R}}^{-1} = \mathbf{r}^T(\mathbf{x}) \mathbf{R}^{-1} \mathbf{R}_{z_d},$$

for any $\mathbf{x} \in \mathcal{X}$.

PROOF. By the definitions of \mathbf{R}_{z_d} and the Woodbury Identity, one has

$$\begin{aligned} \mathbf{R}_{z_d} &= \mathbf{R} - \mathbf{R} \tilde{\mathbf{R}}^{-1} \mathbf{R} = \mathbf{R} \left(\mathbf{I}_n - \left(\mathbf{I}_n + \frac{\lambda_z}{n} \mathbf{R}^{-1} \right)^{-1} \right) \\ &= \mathbf{R} \left(\frac{\lambda_z}{n} \mathbf{R} + \mathbf{I}_n \right)^{-1} = \left(\mathbf{R}^{-1} + \frac{\lambda_z}{n} \mathbf{I}_n \right)^{-1}, \end{aligned}$$

from which (E.1) follows.

Equation (E.2) can be shown similarly by noting $\mathbf{r}_{z_d}^T(\mathbf{x}) = \mathbf{r}^T(\mathbf{x}) - \mathbf{r}^T(\mathbf{x}) \tilde{\mathbf{R}}^{-1} \mathbf{R}$ and the Woodbury Identity. \square

PROOF OF THEOREM 5.1. The predictive mean is as follows

$$\begin{aligned} \hat{\mu}_z(\mathbf{x}) &= \mathbb{E}[y^F(\mathbf{x}) \mid \mathbf{y}^F, \boldsymbol{\theta}, \sigma_0^2, \lambda, \lambda_z] \\ &= f^M(\mathbf{x}, \boldsymbol{\theta}) + \mathbf{r}_{z_d}(\mathbf{x})^T (\mathbf{R}_{z_d} + n\lambda \mathbf{I}_n)^{-1} (\mathbf{y}^F - \mathbf{f}_{\boldsymbol{\theta}}^M) \\ &= f^M(\mathbf{x}, \boldsymbol{\theta}) + \mathbf{r}(\mathbf{x})^T \mathbf{R}^{-1} \mathbf{R}_{z_d} (\mathbf{R}_{z_d} + n\lambda \mathbf{I}_n)^{-1} (\mathbf{y}^F - \mathbf{f}_{\boldsymbol{\theta}}^M) \\ &= f^M(\mathbf{x}, \boldsymbol{\theta}) + \mathbf{r}(\mathbf{x})^T \mathbf{R}^{-1} \left(\mathbf{I}_n + n\lambda \left(\mathbf{R}^{-1} + \frac{\lambda_z}{n} \mathbf{I}_n \right)^{-1} \right) (\mathbf{y}^F - \mathbf{f}_{\boldsymbol{\theta}}^M) \\ &= f^M(\mathbf{x}, \boldsymbol{\theta}) + \frac{\mathbf{r}(\mathbf{x})^T}{(1 + \lambda\lambda_z)} \left(\mathbf{R}^{-1} + \frac{n\lambda}{1 + \lambda\lambda_z} \mathbf{I}_n \right)^{-1} (\mathbf{y}^F - \mathbf{f}_{\boldsymbol{\theta}}^M), \end{aligned}$$

where the last two equalities follow from (E.2) and (E.1), respectively.

The predictive variance can be obtained using (E.2) and (E.1) as follows

$$\begin{aligned} K_z^*(\mathbf{x}, \mathbf{x}) &= K_{z_d}(\mathbf{x}, \mathbf{x}) - \mathbf{r}_{z_d}^T(\mathbf{x}) (\mathbf{R}_{z_d} + n\lambda \mathbf{I}_n)^{-1} \mathbf{r}_{z_d}(\mathbf{x}) \\ &= K(\mathbf{x}, \mathbf{x}) - \mathbf{r}^T(\mathbf{x}) \tilde{\mathbf{R}}^{-1} \mathbf{r}(\mathbf{x}) \\ &\quad - (1 + \lambda\lambda_z)^{-1} \mathbf{r}(\mathbf{x})^T \left(\mathbf{R}^{-1} + \frac{n\lambda}{1 + \lambda\lambda_z} \mathbf{I}_n \right)^{-1} \frac{n}{\lambda_z} \tilde{\mathbf{R}}^{-1} \mathbf{r}(\mathbf{x}) \end{aligned}$$

from which the result follows. \square

PROOF OF LEMMA 5.1. When $\sigma_0^2 = 0$, the predictive mean is as follows

$$\begin{aligned} \mathbb{E}[y^F(\mathbf{x}) \mid \mathbf{y}^F, \boldsymbol{\theta}, \sigma_0^2, \lambda, \lambda_z] &= f^M(\mathbf{x}, \boldsymbol{\theta}) + \mathbf{r}_{z_d}(\mathbf{x})^T \mathbf{R}_{z_d}^{-1} (\mathbf{y}^F - \mathbf{f}_{\boldsymbol{\theta}}^M) \\ &= f^M(\mathbf{x}, \boldsymbol{\theta}) + \mathbf{r}(\mathbf{x})^T \mathbf{R}^{-1} \mathbf{R}_{z_d} \mathbf{R}_{z_d}^{-1} (\mathbf{y}^F - \mathbf{f}_{\boldsymbol{\theta}}^M) \\ &= f^M(\mathbf{x}, \boldsymbol{\theta}) + \mathbf{r}(\mathbf{x})^T \mathbf{R}^{-1} (\mathbf{y}^F - \mathbf{f}_{\boldsymbol{\theta}}^M). \end{aligned}$$

The predictive variance can be obtained similarly. \square

Acknowledgements. The authors thank Dr. Yanxun Xu’s pilot grant for supporting Fangzheng Xie’s research assistantship.

References.

- [1] ANDERSON, K. R. and POLAND, M. P. (2016). Bayesian estimation of magma supply, storage, and eruption rates using a multiphysical volcano model: Kīlauea Volcano, 2000–2012. *Earth and Planetary Science Letters* **447** 161–171.
- [2] ANDERSON, K. R. and POLAND, M. P. (2017). Abundant carbon in the mantle beneath Hawai/i. *Nature Geoscience* **10** 704–708.
- [3] ARENDT, P. D., APLEY, D. W., CHEN, W., LAMB, D. and GORSICH, D. (2012). Improving identifiability in model calibration using multiple responses. *Journal of Mechanical Design* **134** 100909.
- [4] BAYARRI, M. J., BERGER, J. O., PAULO, R., SACKS, J., CAFFEO, J. A., CAVENDISH, J., LIN, C.-H. and TU, J. (2007). A framework for validation of computer models. *Technometrics* **49** 138–154.
- [5] CHENG, H. and SANDU, A. (2010). Collocation least-squares polynomial chaos method. In *Proceedings of the 2010 Spring Simulation Multiconference* 80. Society for Computer Simulation International.
- [6] EDMUNDS, D. E. and TRIEBEL, H. (2008). *Function spaces, entropy numbers, differential operators* **120**. Cambridge University Press.
- [7] GHOSAL, S. and VAN DER VAART, A. (2017). *Fundamentals of nonparametric Bayesian inference* **44**. Cambridge University Press.
- [8] GU, M. (2018a). RobustCalibration: Robust Calibration of Imperfect Mathematical Models R package version 0.5.2.
- [9] GU, M. (2018b). Jointly Robust Prior for Gaussian Stochastic Process in Emulation, Calibration and Variable Selection. *arXiv preprint arXiv:1804.09329*.
- [10] GU, M., PALOMO, J. and BERGER, J. O. (2018). RobustGaSP: Robust Gaussian Stochastic Process Emulation in R. *arXiv preprint arXiv:1801.01874*.
- [11] GU, M. and WANG, L. (2018). Scaled Gaussian stochastic process for computer model calibration and prediction. *arXiv preprint arXiv:1707.08215*.
- [12] GU, M., WANG, X. and BERGER, J. O. (2018). Robust Gaussian Stochastic Process Emulation. *Annals of Statistics, In Press*. *arXiv preprint arXiv:1708.04738*.
- [13] HANDCOCK, M. S. and STEIN, M. L. (1993). A Bayesian analysis of kriging. *Technometrics* **35** 403–410.
- [14] HODGES, J. S. and REICH, B. J. (2010). Adding spatially-correlated errors can mess up the fixed effect you love. *The American Statistician* **64** 325–334.
- [15] KENNEDY, M. C. and O’HAGAN, A. (2001). Bayesian calibration of computer models. *Journal of the Royal Statistical Society: Series B (Statistical Methodology)* **63** 425–464.
- [16] KOSOROK, M. R. (2008). *Introduction to empirical processes and semiparametric inference*. Springer.
- [17] MAMMEN, E. and VAN DE GEER, S. (1997). Penalized quasi-likelihood estimation in partial linear models. *The Annals of Statistics* 1014–1035.
- [18] MOROKOFF, W. J. and CAFLISCH, R. E. (1995). Quasi-monte carlo integration. *Journal of computational physics* **122** 218–230.
- [19] NOCEDAL, J. (1980). Updating quasi-Newton matrices with limited storage. *Mathematics of computation* **35** 773–782.
- [20] PINELIS, I. (1994). Optimum bounds for the distributions of martingales in Banach spaces. *The Annals of Probability* 1679–1706.

- [21] RASMUSSEN, C. E. (2006). *Gaussian processes for machine learning*. MIT Press.
- [22] REICH, B. J., HODGES, J. S. and ZADNIK, V. (2006). Effects of residual smoothing on the posterior of the fixed effects in disease-mapping models. *Biometrics* **62** 1197–1206.
- [23] RUDELSON, M., VERSHYNIN, R. et al. (2013). Hanson-Wright inequality and subgaussian concentration. *Electronic Communications in Probability* **18**.
- [24] SANTNER, T. J., WILLIAMS, B. J. and NOTZ, W. I. (2003). *The design and analysis of computer experiments*. Springer Science & Business Media.
- [25] SURJANOVIC, S. and BINGHAM, D. (2017). Virtual Library of Simulation Experiments: Test Functions and Datasets. <http://www.sfu.ca/~ssurjano>.
- [26] TUO, R. and WU, C. J. (2015). Efficient calibration for imperfect computer models. *The Annals of Statistics* **43** 2331–2352.
- [27] TUO, R. and WU, C. J. (2016). A theoretical framework for calibration in computer models: parametrization, estimation and convergence properties. *SIAM/ASA Journal on Uncertainty Quantification* **4** 767–795.
- [28] VAN DE GEER, S. A. (2000). *Empirical Processes in M-estimation* **6**. Cambridge university press.
- [29] VAN DER VAART, A. W. (2000). *Asymptotic statistics* **3**. Cambridge university press.
- [30] WAHBA, G. (1990). *Spline models for observational data* **59**. Siam.
- [31] WONG, R. K., STORLIE, C. B. and LEE, T. (2017). A frequentist approach to computer model calibration. *Journal of the Royal Statistical Society: Series B (Statistical Methodology)* **79** 635–648.
- [32] XIE, F. and XU, Y. (2018). Bayesian Projected Calibration of Computer Models. *arXiv preprint arXiv:1803.01231*.
- [33] XIONG, S., QIAN, P. Z. and WU, C. J. (2013). Sequential design and analysis of high-accuracy and low-accuracy computer codes. *Technometrics* **55** 37–46.
- [34] YANG, Y., BHATTACHARYA, A. and PATI, D. (2017). Frequentist coverage and sup-norm convergence rate in Gaussian process regression. *arXiv preprint arXiv:1708.04753*.
- [35] YANG, Y. and PATI, D. (2017). Bayesian model selection consistency and oracle inequality with intractable marginal likelihood. *arXiv preprint arXiv:1701.00311*.
- [36] YANG, Y., SHANG, Z. and CHENG, G. (2017). Non-asymptotic theory for nonparametric testing. *arXiv preprint arXiv:1702.01330*.
- [37] ZHANG, H. (2004). Inconsistent estimation and asymptotically equal interpolations in model-based geostatistics. *Journal of the American Statistical Association* **99** 250–261.
- [38] ZHANG, H. and ZIMMERMAN, D. L. (2005). Towards reconciling two asymptotic frameworks in spatial statistics. *Biometrika* **92** 921–936.

MENGYANG GU
 FANGZHENG XIE
 LONG WANG
 DEPARTMENT OF APPLIED MATHEMATICS AND STATISTICS
 JOHNS HOPKINS UNIVERSITY,
 3400 NORTH CHARLES STREET, WHITEHEAD HALL 100,
 BALTIMORE, MARYLAND, 21218-2608
 USA
 E-MAIL: mgu6@jhu.edu
fxie5@jhu.edu
lwang100@jhu.edu